

The Pennsylvania State University
The Graduate School
Department of Materials Science and Engineering

GROWTH OF EuO THIN FILMS by MOLECULAR BEAM EPITAXY

A Thesis in
Materials Science and Engineering

By
Ross W. Ulbricht

© 2009 Ross W. Ulbricht

Submitted in Partial Fulfillment
of the Requirements
for the Degree of

Master of Science

May 2009

This thesis of Ross W. Ulbricht was reviewed and approved* by the following:

Darrell G. Schlom

Professor of Materials Science and Engineering

Thesis Adviser

Venkatraman Gopalan

Professor of Materials Science and Engineering

Xiaoxing Xi

Professor of Physics and Materials Science and Engineering

Joan Redwing

Professor of Materials Science and Engineering

Head of the Department of Materials Science and Engineering

*Signatures are on file with the Graduate School.

ABSTRACT

The highly spin polarized ferromagnetic semiconductor, EuO is being examined as a candidate material for spintronics applications. Its development in this role has been stifled, however, by difficulties in synthesizing high quality, epitaxial thin-films. Using molecular-beam epitaxy, these difficulties have been overcome and the adsorption-controlled growth of epitaxial EuO films on single crystalline (110) YAlO₃ substrates has been demonstrated. The optimal substrate temperature and oxygen background partial pressure for the growth of high quality EuO have been determined to be 590 °C and 1×10^{-9} torr, respectively. Four-circle x-ray diffraction (XRD) reveals phase-pure, epitaxial, (001)-oriented films with rocking curve full width at half maxima as narrow as 34 arc seconds (0.0097°). Off-axis XRD analysis shows that the unit cell of the EuO film is rotated by 45° with respect to the surface net of the (110) YAlO₃ substrate, inducing an ~2%, in-plane tensile strain in commensurate films due to lattice mismatch. The critical thickness for the onset of relaxation of (001) EuO on (110) YAlO₃ was determined from XRD measurements in combination with Rutherford backscattering spectrometry (RBS) to be 382 ± 25 Å. A saturation magnetization of 6.96 ± 0.07 μ_B /Eu, a value close to the theoretical limit of 7 μ_B /Eu, was measured on these epitaxial EuO films using a superconducting quantum interference device (SQUID) magnetometer.

TABLE OF CONTENTS

LIST OF FIGURES	v
Chapter 1: Background	1
1.1 Introduction	1
1.2 Crystal structure of EuO	2
1.3 Phases of EuO	4
1.4 Molecular-beam epitaxy of oxides	6
1.5 Adsorption-controlled growth	8
1.6 Thin films of EuO	10
1.6.1 Growth	10
1.6.2 Properties	15
Chapter 2: Adsorption-controlled growth	19
2.1 Introduction	19
2.2 Adsorption controlled growth regime	21
2.3 Experimental procedure	21
2.3.1 Seed crystal	21
2.3.2 Growth parameters	22
2.4 Results and discussion	25
2.4.1 X-ray diffraction	25
2.4.2 Reflection High-Energy Electron Diffraction (RHEED)	28
2.4.3 Oxygen flux dependence	30
2.4.4 Strain relaxation	30
2.4.5 Magnetic properties	36
2.5 Conclusions	36
Chapter 3: Alternative substrates	40
3.1 Introduction	40
3.2 Lanthanum Aluminate	40
3.3 Yttria Stabilized Zirconia	45
3.4 Sapphire	49
3.5 Diamond	49
Chapter 4: Conclusions and future direction	58
REFERENCES	60

LIST OF FIGURES

Figure 1.1 Crystal structure of EuO

Figure 1.2 Oxygen-fugacity vs. temperature for the europium-oxygen system

Figure 1.3 Schematic of MBE chamber

Figure 1.4 Reaction equilibrium curves for GaAs and PbTiO₃

Table 1.1 Epitaxial growth of EuO on various substrates

Figure 1.5 Magnetic hysteresis and saturation of EuO

Figure 1.6 Adsorption vs. temperature for EuO

Figure 2.1 Crystal structure of YAlO₃

Figure 2.2 Epitaxial relationship between EuO and YAlO₃

Figure 2.3 X-ray diffraction scans of EuO

Figure 2.4 Surface net alignment of EuO on YAlO₃

Figure 2.5 RHEED patterns of EuO and YAlO₃

Figure 2.6 Thickness vs. oxygen partial pressure showing adsorption growth of EuO

Figure 2.7 EuO rocking curves showing film relaxation

Figure 2.8 Rocking curve FWHM vs. film thickness showing relaxation of EuO

Figure 2.9 Magnetization vs. temperature showing ferromagnetic transition of EuO

Figure 2.10 Magnetic hysteresis of EuO

Table 3.1 Growth conditions for various substrates used to grow EuO

Figure 3.1 Epitaxial alignment between EuO and LaAlO₃

Figure 3.2 Magnetization vs. temperature of EuO on LaAlO₃

Figure 3.3 RHEED patterns of EuO and LaAlO₃

Figure 3.4 Epitaxial alignment of YSZ, SrO and EuO

Figure 3.5 $\theta - 2\theta$ x-ray diffraction scan of YSZ // SrO // EuO

Figure 3.6 RHEED patterns of YSZ, SrO and EuO

Figure 3.7 Surface net of $(1\bar{1}02)$ Al_2O_3

Figure 3.8 RHEED patterns of EuO and Al_2O_3

Figure 3.9 XRD pattern of EuO and Al_2O_3

Figure 3.10 Out-of-plane x-ray diffraction of EuO grown on diamond

Figure 3.11 In-plane x-ray diffraction of EuO grown on diamond

Figure 3.12 RHEED patterns of EuO and diamond

Chapter 1: Background

1.1 Introduction

A material of choice often defines an historical era. The Stone Age and the Bronze Age are examples of this. In modern times, nearly all materials have been revolutionized. Advances in one field have led to advances in others with many previously disparate fields overlapping as fundamental understanding increases and deep commonalities are found. In many ways, materials science is a melting pot of academic disciplines like chemistry, thermodynamics and solid-state physics. A large portion of materials science focuses on the solid state where the arrangement of atoms and the interaction of their electrons lead to a myriad of intricate physical properties. Besides glass and some polymers, solids typically take a crystalline form where atoms are arranged with periodic uniformity. It is often in crystals where the most pronounced and interesting properties arise.

Advances in computational power and techniques have led to a tremendous amount of effort directed toward modeling material systems and crystals in particular. From computer models, one can derive the properties that certain crystal systems are likely to exhibit. By predicting crystal properties, scientists can greatly narrow their focus to materials that are at least likely to have the properties they desire. It is then the task of experimentalists to fabricate a crystal as nearly identical to the crystal modeled and determine whether the properties it was predicted to have are indeed present. One such system of tremendous potential is the EuO crystal, which is the focus of this thesis.

There are many crystal growth methods, each with their own pros and cons that produce crystals of varying quality. Some methods are used to produce single crystals, which are stand alone crystals of a single phase in which the atoms are arranged in a regular repeating arrangement such as those found naturally in the earth like quartz or diamond. Others methods produce crystalline thin films. Thin films can be grown on top of a preexisting single crystal that has a similar atomic spacing in order to enable the depositing species to extend the single crystal lattice into the deposited film, a process known as epitaxy. Epitaxial thin films are often used in technological applications and allow for control of many aspects of crystal growth such as strain and orientation. In this thesis, the molecular-beam epitaxy (MBE) crystal growth method is utilized. MBE is one of the most precise methods in use today and can be used to make nearly perfect crystalline thin films.

This thesis details the latest growth technique that has been applied to the growth of EuO called adsorption-controlled growth. This technique has been used to grow stoichiometric EuO thin films of the highest quality yet reported.

1.2 Crystal structure of EuO

EuO takes the rocksalt crystal structure, which is characterized by alternating europium and oxygen atoms in each of the three dimensions on a face centered cubic (FCC) lattice. EuO has a europium and an oxygen atom for each lattice point with oxygen shifted by half of a unit cell in one direction (see figure 1.1). At room temperature, EuO has a lattice constant of 5.144 Å, putting the interatomic distance of

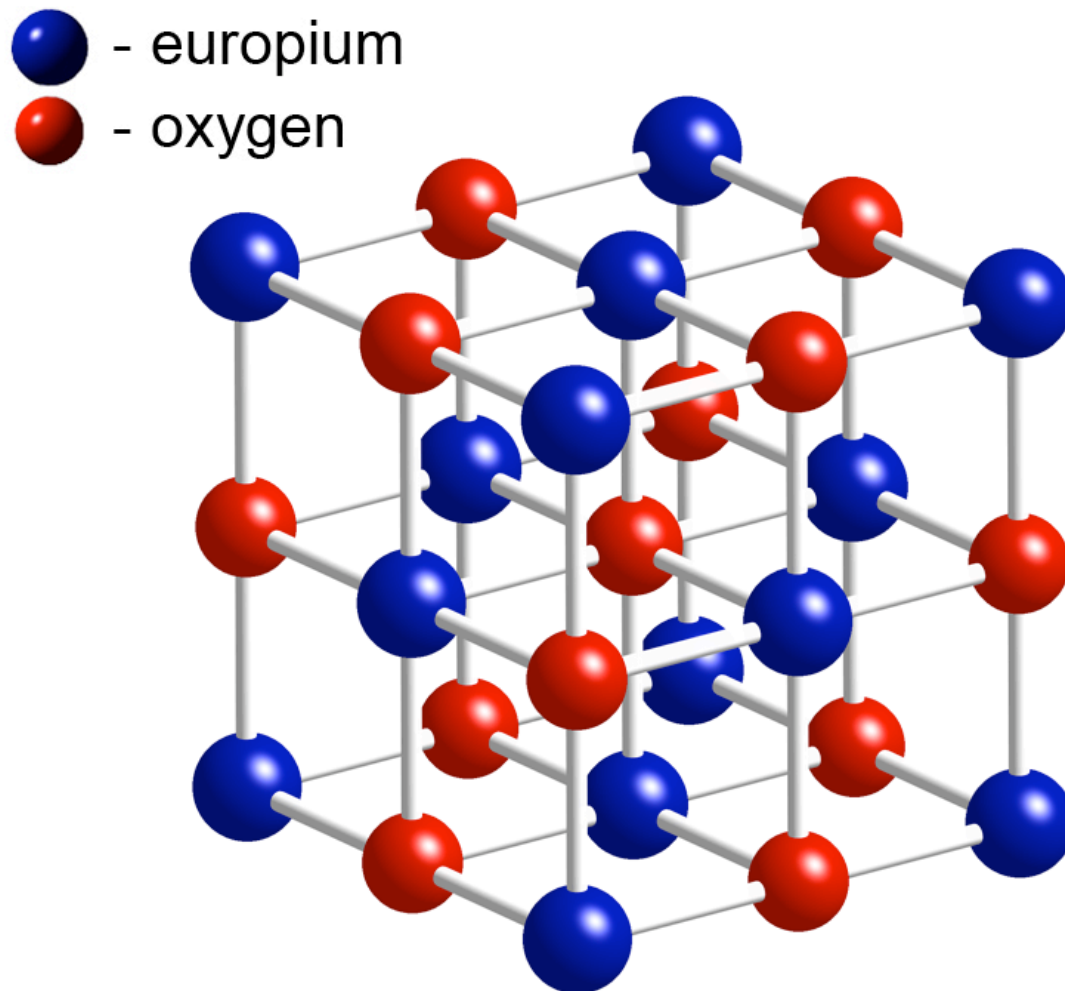


Fig. 1.1. EuO single crystal unit cell displaying the cubic symmetry of its rocksalt structure. Surprisingly, there is a higher density of europium atoms in EuO than in europium metal because europium metal takes the body centered cubic structure while the europium sublattice in EuO is face centered cubic which has a higher packing density even with the additional oxygen atoms in the structure.

nearest neighbor atoms at 2.572 Å. Below 10 K, this is reduced to 5.127 Å.¹ Europium metal takes the body centered cubic (BCC) crystal structure, which is not as closely packed as an FCC lattice. Even though there are oxygen atoms taking up space in EuO, the tighter packing of the FCC europium sublattice makes the density of europium atoms higher in EuO than in Eu metal. EuO is an ionic crystal with Eu^{2+} being the cation and O^{2-} being the anion, giving europium an electron configuration of $[\text{Xe}]4f^7$. This half filled valence $4f$ electron orbital gives rise to EuO having many unique properties. These properties will be discussed later in this chapter.

1.3 Phases of EuO

Figure 1.2 depicts the oxygen-fugacity vs. temperature ($f_{\text{O}_2}(T)$) diagram as presented by McCarthy and White for the europium – oxygen system.² This diagram depicts the boundaries between the three europium oxide compounds EuO, Eu_3O_4 , and Eu_2O_3 in $\log f_{\text{O}_2}(T)$ space. $\log f_{\text{O}_2}(T)$ is given by the function, $\log f_{\text{O}_2}(T) = \Delta G^\circ(T)/4.576T$ where $\Delta G^\circ(T)$ is the free energy change per mole of O_2 as a function of temperature T (in K). This oxygen-fugacity vs. temperature diagram can be used as a guide to the oxidation-reduction stability among the europium oxides and shows that the optimal oxygen partial pressure for EuO growth must be very low. Experimentally, the oxygen partial pressures needed for EuO formation often approach the lower limit of laboratory equipment as will be seen in chapter 2 of this thesis.

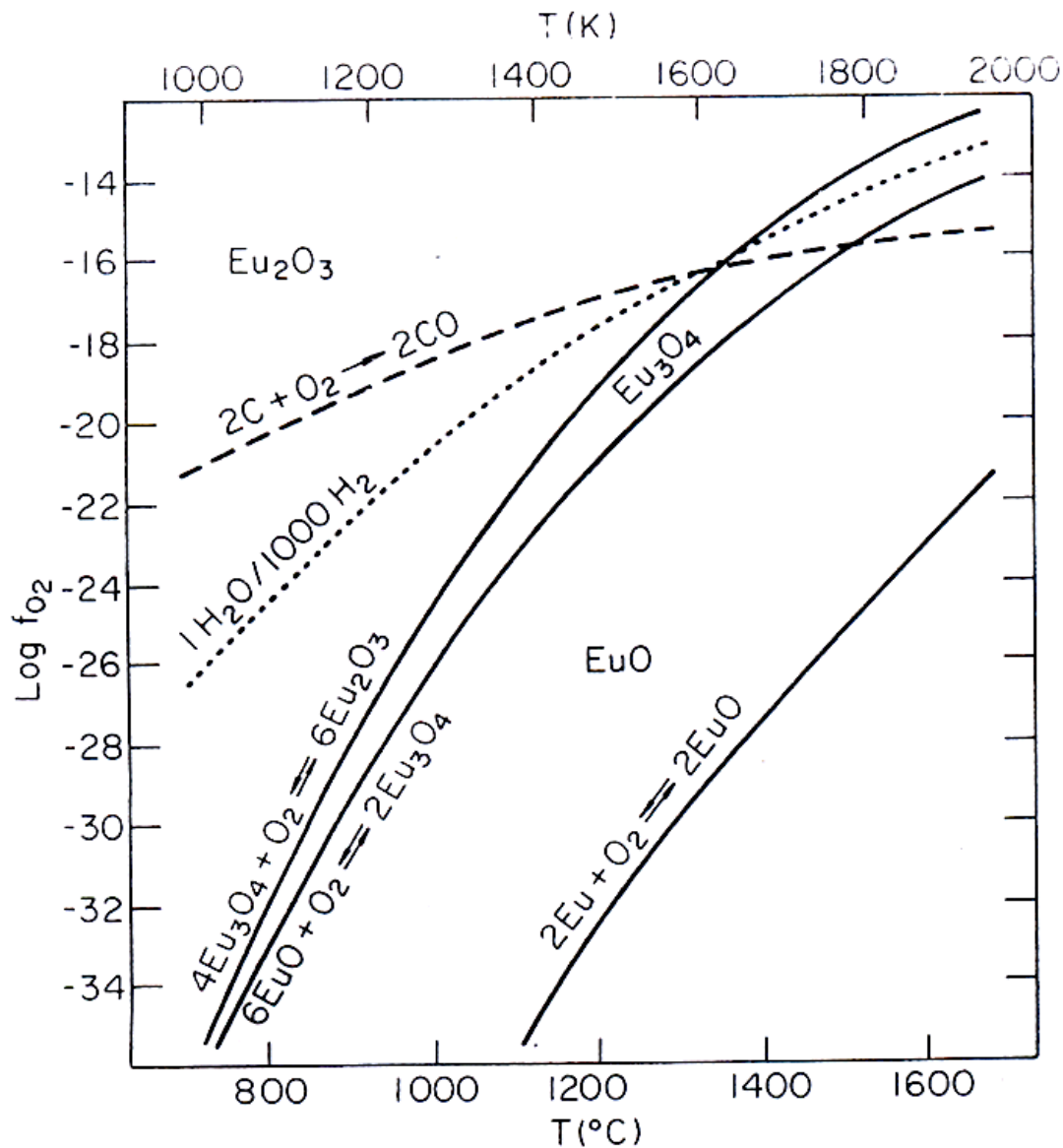


Figure 1.2. Oxygen-fugacity vs. temperature ($f_{O_2}(T)$) diagram for the europium – oxygen system.² The optimal oxygen partial pressure needed for the formation of EuO can be seen to be very low in comparison to the higher oxidation states of europium oxide.

1.4 Molecular-beam epitaxy of oxides

Molecular-beam epitaxy (MBE) is a versatile technique for growing high quality crystalline thin films. Though originally developed and used for growth of semiconductor compounds such as GaAs,³ its use has expanded to the growth of oxide thin films where its precise control has been used to create complex oxide structures not found in nature or attainable to date by other crystal growth methods.⁴ In oxide MBE, molecular beams comprised of different elements travel through ultra-high vacuum (UHV) and react with one another and oxygen on a substrate surface to form a crystalline thin film. Beams are formed instead of clouds because the mean free path of the atoms in the beam is significantly longer than the dimensions of the vacuum chamber in which the crystal is grown because of the UHV conditions of the chamber. Figure 1.3 shows a schematic of an MBE system. Effusion cells housing the constituent elements of the desired film are heated until the desired vapor pressure is attained for each element as measured by a quartz crystal microbalance (QCM). The QCM measures the deposition rate from the beam of atoms by detecting the rate of change in its vibration frequency due to increased mass from the incident beam atoms. Typical growth rates for thin films grown by MBE are on the order of 1 monolayer/minute. This is slow enough that surface migration of the incident atoms and their integration into the growing crystal lattice is allowed.

Crystal growth in MBE is often monitored in situ using reflection high-energy electron diffraction (RHEED). Under the UHV conditions of MBE, a beam of high-energy electrons with a wavelength of $\sim 0.1 \text{ \AA}$ can be directed at the growing film at a low incident angle. Because of the low angle, the penetration of the beam into the crystal is

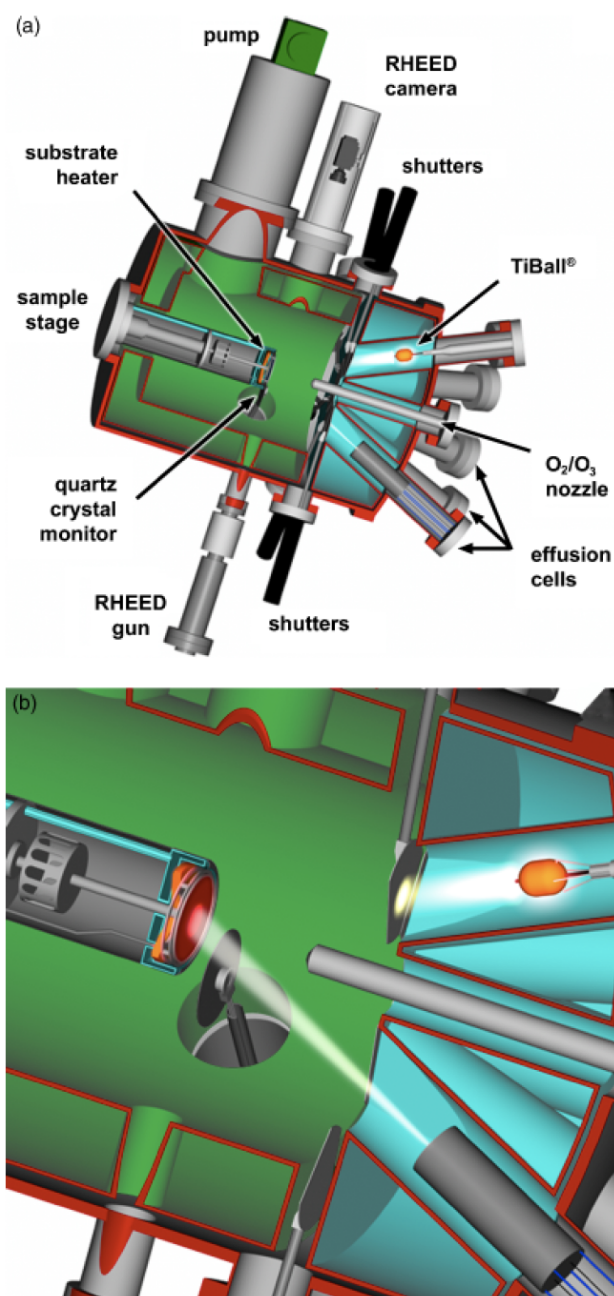


Figure 1.3. Schematic of MBE chamber.⁵ Background pressures lower than 10^{-8} torr. Effusion cells house pure elements that, when heated, emit beams that combine and crystallize on a substrate at the center of the chamber. Crystal diffraction patterns are monitored in real-time as the crystal is grown using reflection high energy electron diffraction (RHEED).

limited to the first few atomic layers. The reflected beam is imaged upon a fluorescent screen and reveals the crystalline character of the film surface. Electrons in the RHEED beam have a wavelength comparable to the three-dimensional diffraction grating created by the atoms in a thin film. They therefore create interference patterns in the reflected beam that are in essence a reciprocal space map of the crystal structure they have reflected off of. This gives helpful clues to the MBE crystal grower for the suitability of chamber conditions to crystal growth.

1.5 Adsorption-controlled growth

An inherent problem with the crystal growth of multi-component materials by MBE is maintaining stoichiometry within the growing crystal. This becomes especially difficult for compounds with many elements. Assuming all atoms from the beams incident on the substrate stick and are incorporated into the growing crystal, one must precisely control the flux of all incident beams relative to one another to ensure stoichiometry in the resultant film. However, the different atoms in the film's composition as well as the various compounds they can produce in combination will stick to the substrate with differing degrees at different substrate temperatures, thus adding another element of difficulty to creating stoichiometric films. However, this fact offers an opportunity for a different kind of growth regime that avoids flux matching altogether. Because of the varying vapor pressures of the various elements and compounds impinging upon the substrate, there may, in some cases, exist a substrate temperature where the desired compound will have a vapor pressure lower than its constituents and will therefore stick to the substrate while any excess high vapor pressure material (i.e.,

that of the constituents) will simply desorb leaving a film of the stoichiometric low vapor pressure material.

This adsorption-controlled MBE regime was first used to grow GaAs in 1968.³ Arsenic has a much higher vapor pressure over solid arsenic than it does over solid GaAs. Thus, GaAs will be stable and there will be no net loss of arsenic from the growing GaAs film so long as the incident flux of arsenic is greater than the flux of arsenic being desorbed from the GaAs at the substrate temperature used for growth due to the vapor pressure of arsenic over GaAs. When the incident arsenic flux becomes so high that it corresponds to the vapor pressure of arsenic over solid arsenic, then solid arsenic also begins to accumulate in the depositing film. But between these two arsenic fluxes exists a region (the “growth window”) where single-phase GaAs can be grown by adsorption-controlled growth. Figure 1.4 shows this growth window in terms of gas pressure and temperature for GaAs and PbTiO_3 .⁶ Above the upper dotted line, solid arsenic forms. Between the dotted lines, solid GaAs forms with excess arsenic gas evaporating away. Below the lower dotted line, the solid GaAs decomposes into liquid gallium and arsenic gas.

Later, adsorption controlled growth was utilized to grow complex oxide structures by MBE. Two examples are PbTiO_3 and $\text{Bi}_4\text{Ti}_3\text{O}_{12}$.^{6,7} In both cases, the A-site cations (lead and bismuth) and oxygen are supplied in excess many times greater than their stoichiometric ratios. These elements combine to create binary metal oxides (PbO and Bi_2O_3) that have vapor pressures well in excess of the relevant oxide under the growth conditions for titanium, TiO_2 . Therefore, at a temperature above which all incident PbO , in the case of PbTiO_3 , will evaporate, an overpressure of lead and oxygen will allow the

growth rate of PbTiO_3 to be controlled entirely by the titanium flux since any PbO remaining after all titanium has reacted and been incorporated into the film will evaporate away. The growth window for PbTiO_3 is shown in figure 1.4. This window is much narrower than that of GaAs , but is still wide enough and within a suitable temperature and pressure range for MBE growth.⁴ Above the solid upper line, solid PbO forms. Between the solid lines, PbTiO_3 forms with excess PbO gas evaporating away. Below the solid lower line, all lead is evaporated away as PbO gas and solid TiO_2 remains.

The use of adsorption controlled growth of EuO was first proposed by Steeneken et al.⁸ Europium metal was deposited on a cooling EuO film while measuring its surface conductivity. At temperatures below 340°C the surface conductivity began increasing linearly. This was likely due to europium metal accumulating on the surface of the film, thus making a conductive pathway. Above this temperature, the conductivity was the same as a pure EuO film indicating that the incident europium metal was probably being evaporated. This indicated that the adsorption controlled growth regime is likely above 340°C . The adsorption controlled growth window for EuO is more conclusively determined later in this thesis.

1.6 Thin films of EuO

1.6.1 Growth

EuO was first created in 1961 as a single crystal,⁹ but it wasn't until 1967 that the first EuO thin film was grown.¹⁰ Though this and many later studies were conducted with polycrystalline thin films, insight into the thin-film properties of EuO were still gleaned. These films were deposited using a variety of techniques including rf

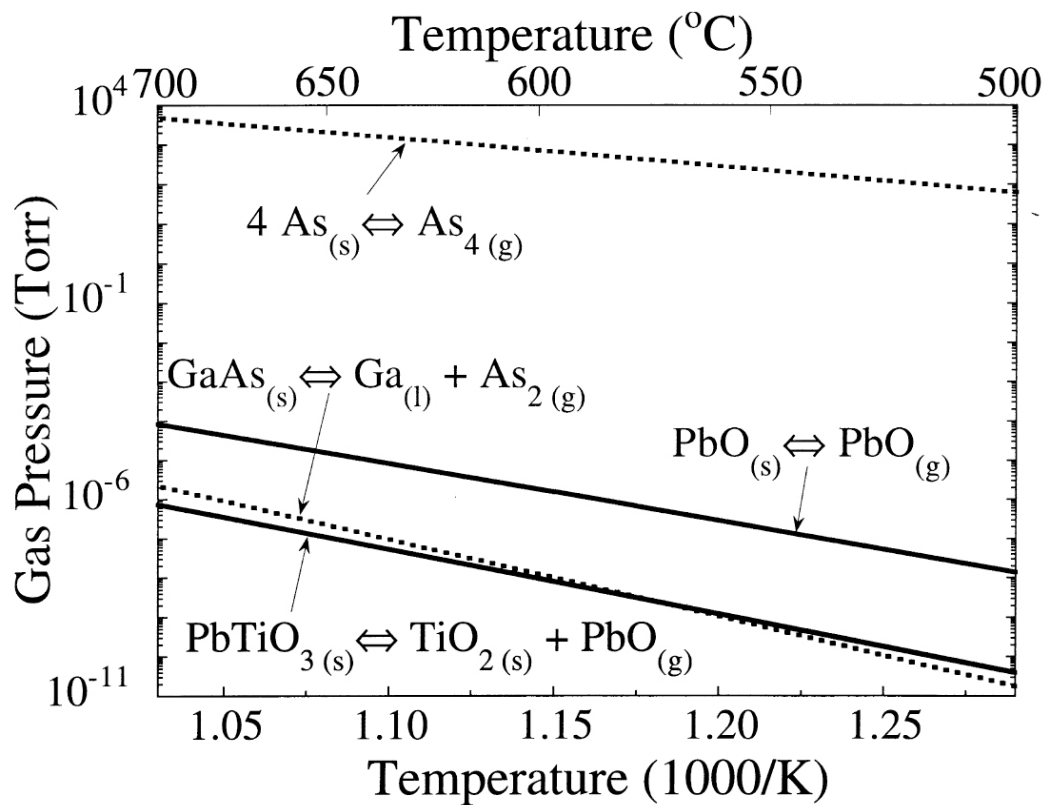


Figure 1.4. Reaction equilibrium curves for GaAs (dotted lines) and PbTiO₃ (solid lines).

The adsorption-controlled growth window for each compound lies between its corresponding lines where it is stable and any excess material is evaporated away as a high vapor pressure gas.⁶

sputtering,¹¹ evaporation of europium metal in a high partial pressure of oxygen, electron beam heating of bulk EuO, co-deposition of europium and Eu₂O₃,¹⁰ Molecular-beam epitaxy,¹² and even sol-gel,¹³ just to name a few. Initially, EuO films were grown by oxidizing preexisting europium metal films in 10⁻³ torr oxygen pressure at 200 °C.¹⁰ While this method succeeded in producing EuO films, they were of low quality and at 800 Å thick, likely not to be uniform. A few years later, another method was reported that would eventually lead to the technique used in recent years. Instead of attempting to oxidize an already grown europium film, europium metal and Eu₂O₃ were simultaneously evaporated from an effusion cell and by an electron beam respectively. Thus, europium and oxygen were allowed to react in the growing film and produce a more uniform film. Stoichiometry could be controlled with this method because the europium and Eu₂O₃ fluxes could be adjusted relative to one another. By the end of the second millennium, MBE technology had advanced and a new growth method for EuO was reported. Drawing from the flux matching technique, europium and pure oxygen were matched in a growing EuO film at roughly 3×10¹³ at/cm²/s corresponding to a very low 2.2×10⁻⁹ torr partial pressure of oxygen.¹⁴

This thesis, however, focuses on the epitaxial growth of EuO where the entire film is of a single crystallographic orientation. The orientation of epitaxial films is heavily influenced by the orientation of the substrate on which they are grown. Also, if there is a mismatch in the lattice spacing of the substrate and the film, a bi-axial strain can be induced in the film so long as it does not grow beyond a thickness where it begins to relax called its critical thickness. Prior to the onset of relaxation, the film is called “coherent.”

Table 1 summarizes the various substrates that have been used to grow epitaxial EuO thin films along with their relative orientation and lattice mismatch to EuO. An obvious substrate choice for EuO is yttria stabilized zirconia (YSZ) because it has a lattice spacing nearly identical to EuO. ZrO_2 alone has monoclinic crystal structure, but with the addition of yttrium, it can be stabilized in a cubic structure. This choice of substrate has one major drawback, however. YSZ acts as an oxygen donor and will transform EuO into one or both of its higher oxidation states (Eu_2O_3 and Eu_3O_4).¹⁹ A description of a solution to this challenge can be found in section 3.1 of this thesis. (100) SrTiO_3 and (100) MgO were also used to grow epitaxial (100) EuO thin films, though both suffer from large lattice mismatches with EuO resulting in relaxed films containing many defects. SrTiO_3 also over oxidizes EuO in the same way as YSZ.¹⁵ In 2003 EuO was successfully integrated epitaxially with silicon.¹⁹ Though silicon is not an ideal substrate in terms of lattice spacing or composition, this was an important step in the development of EuO as a potential material for high tech application as silicon is ubiquitous in this industry. Silicon poses an interesting challenge, however, as the oxygen partial pressures needed to grow EuO will also oxidize silicon leaving a SiO_2 template for the EuO film instead of the desired pure silicon template. It is therefore necessary to simultaneously ramp up the europium and oxygen fluxes by the same amount when initiating growth. This could be avoided with the aforementioned oxide substrates because oxygen flux could be set first without fear of oxidizing the substrate. Growth of EuO on (110) YAlO_3 , (1 $\bar{1}$ 02) Al_2O_3 , (001) diamond, and (001) LaAlO_3 will be discussed in chapter 3.

year	substrate	substrate orientation	EuO orientation	lattice mismatch [†]	reference
1970	CaF ₂	(111)	(111)	6.3%	11
1994	YSZ [‡]	(001)	(001)	0%	33
2000	MgO	(001)	(001)	-18.1%	15
2000	SrTiO ₃	(001)	(001)	7.3%	15
		[100]	[110]		
2003	Si	(001)	(001)	5.7%	29
2007	GaN	(001)	(111)	-12.3%	19
2007	YAlO ₃	(110)	(001)	2.2%	19
		[001]	[110]		
2008	Al ₂ O ₃	(1 $\bar{1}$ 02)	(100)	-4%	*
2008	diamond	(001)	(001)	-2.1%	*
		[100]	[110]		
2008	LaAlO ₃	(001)	(001)	4%	*

Table 1.1. Epitaxial growth of EuO on various substrates. Orientations are out-of-plane unless a second is given in which case the second is in-plane. If only one is given, it is assumed that the in-plane orientations are identical for film and substrate.

[†]Lattice mismatch (Δa) is calculated with the following equation: $\Delta a = (a_s - a_f) / a_f$

where a_s is the substrate lattice constant and a_f is the film lattice constant, in this case EuO with $a_f = 5.14 \text{ \AA}$.

[‡]Yttria stabilized zirconia (YSZ) is ZrO₂ with enough yttrium substituted into the zirconium sublattice to stabilize the crystal structure in cubic symmetry.

*Presented in this thesis

1.6.2 Properties

The properties of EuO are many and varied, and in some cases, quite exceptional. Most oxides that contain magnetic ions are antiferromagnetic. EuO is a rare exception and is a ferromagnet with a Curie temperature (T_c) around 69 K.¹⁰ As a 2+ ion in EuO, Eu has an f valence orbital half filled with electrons. Due to a large spin state energy splitting, the spin of these electrons is parallel and contributes to a net magnetic moment of $7 \mu_B$ per europium atom in the ideal case. This is the highest possible value for any known element because elements with orbitals higher than f have not been found in nature. High degrees of magnetization have been achieved in both single crystals and thin films with some reports as high as 98.6%¹⁵ (see figure 1.5). In section 2.3.2 a growth technique is described that produces thin films with the highest magnetization yet reported for EuO. Ferromagnetism is most often found in metals where the exchange interaction of free electrons leads to magnetic order. EuO is, however, a semiconductor with a band gap of 1.12 eV.⁸ Typically, magnetic ordering in semiconductors or insulators such as FeO is governed by super exchange, which leads to anti-ferromagnetic ordering. However, under the Heisenberg ferromagnet description, a ferromagnetic semiconductor is possible and it was its realization in EuO that helped EuO garner much interest.

EuO's magneto optical properties are among the largest known, with a Faraday rotation of 7.5×10^5 °/cm.¹⁶ Upon transition into the ferromagnetic phase, or when an

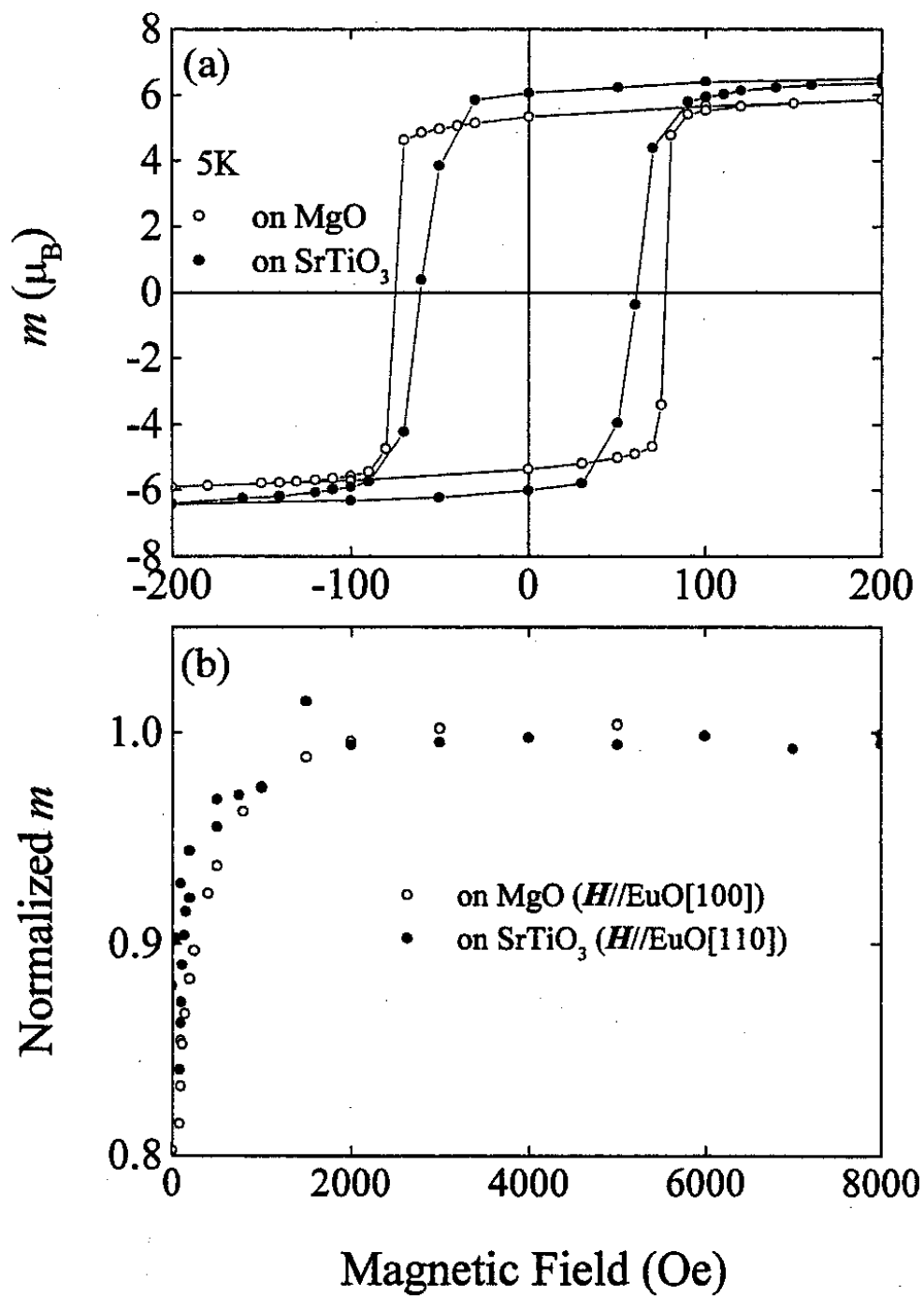


Figure 1.5. (a) Ferromagnetic hysteresis curves for EuO grown on MgO and SrTiO₃. (b) Magnetization of EuO under saturating magnetic fields. The vertical axis is normalized to the theoretical limit of magnetization in EuO.¹⁵

external magnetic field is applied to it, the band gap in EuO shrinks by about 0.3 eV.⁸

When the valence $4f$ electrons polarize, through the direct exchange interaction with the conduction electrons, the conduction band splits into spin up and spin down levels, which differ by 0.6 eV.¹⁹ This reduces its band gap as can be seen in a shift lower in its optical adsorption edge in Fig. 1.6 and results in EuO having nearly 100% spin polarized electrons, making it a half-metal.⁸ EuO also exhibits a large metal to insulator transition with reports of resistivity changes exceeding 8 orders of magnitude.¹⁷

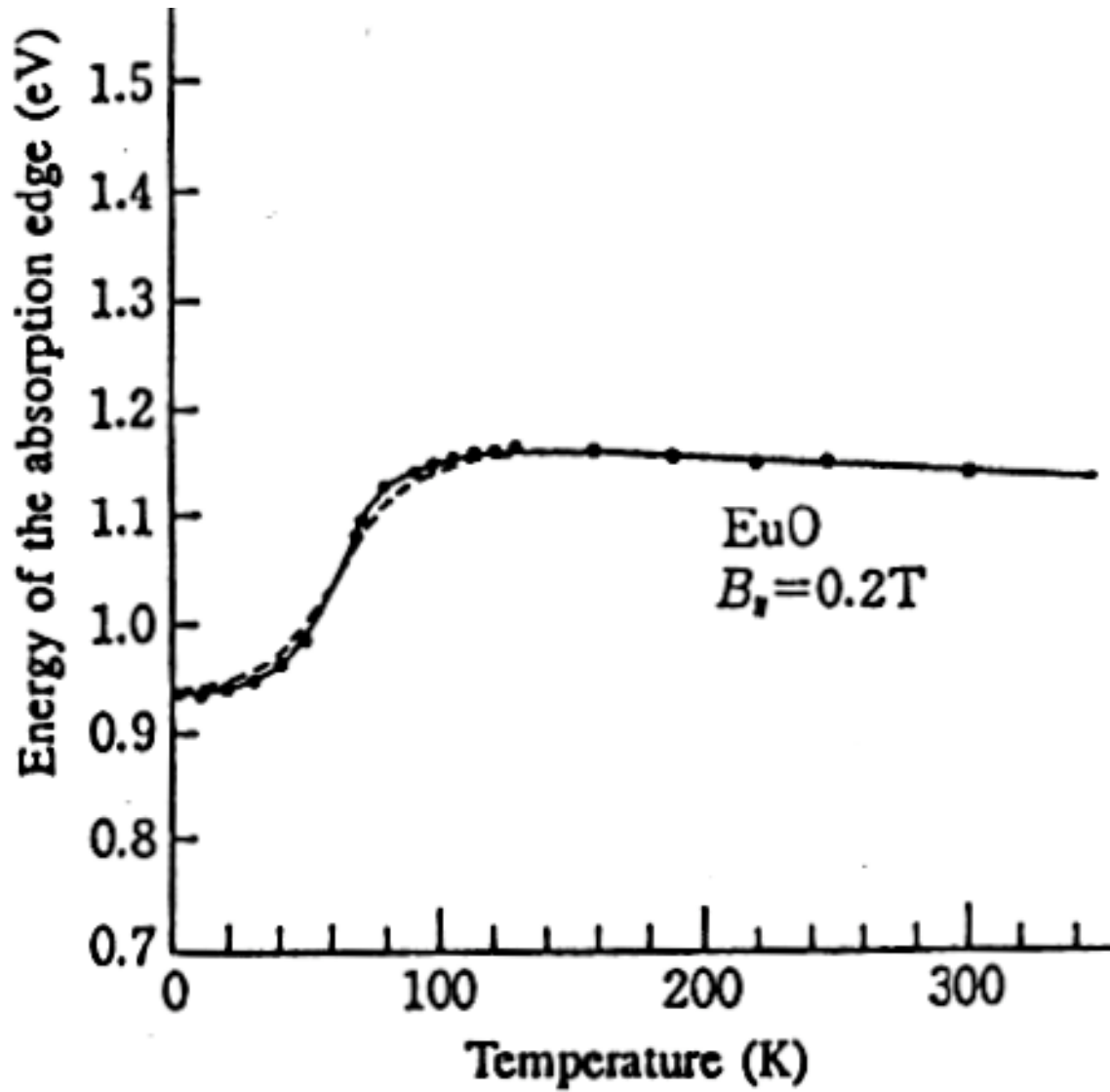


Figure 1.6. Absorption edge shift of EuO around its ferromagnetic transition temperature, 69 K.¹⁸

Chapter 2: Adsorption-controlled growth

2.1 Introduction

With a spin polarization exceeding 90% and its ability to be epitaxially integrated with mainstream, long spin lifetime semiconductors such as silicon and GaN,¹⁹ the ferromagnetic semiconductor EuO is an attractive material for semiconductor-based spintronic devices. In the ferromagnetic phase ($T_C = 69$ K), the $4f^7$ electron configuration of Eu^{2+} induces a magnetic moment of $7 \mu_B$ per europium atom. This, together with a density of europium atoms that exceeds that of europium metal, makes EuO one of the strongest known ferromagnets.⁸ Additionally, it has outstanding magneto-optical properties, with a Faraday rotation of 8.5×10^5 °/cm in a field of 2 T.²⁰ It shows colossal magneto-resistance²¹ and, if appropriately doped, a metal to insulator transition with a resistance change that exceeds 13 orders of magnitude.²² This renders EuO a very attractive material for basic and device oriented research.

Above its relatively low ferromagnetic transition temperature of 69K, EuO is rendered useless for spintronics applications because the spin polarization that is the source of its ferromagnetism is lost to entropy and without spin polarization, the spin direction in the material is indistinct. Despite this, a better understanding of its properties might provide insight into its potential for spintronics applications. It has been predicted that compressive biaxial strain can increase the ferromagnetic transition temperature of EuO by as much as 30%. If this effect can be combined with the amplifying effect doping has on the transition temperature, EuO's ferromagnetism may be assessable near room temperature.³⁹ A ferromagnetic transition temperature of 170 K has been observed

in gadolinium doped EuO.²³ If strained, gadolinium doped EuO could have a transition temperature of 221 K.

EuO has been studied extensively as a single crystal²¹⁻²⁵ and as a thin film,^{8, 19,20,26-29} but as a commensurate, epitaxially grown thin film, there is much to be understood about its behavior and films with high structural quality have not, until now, been fabricated. Interest in EuO was first generated by its remarkable properties and for several decades starting in the 1960's single crystals were grown and its various properties were investigated. EuO was also studied as a polycrystalline and epitaxial thin-film. EuO thin films share the same basic properties of EuO single crystals such as ferromagnetism but are markedly different, for example, in their transport properties. Unlike EuO single crystals, resistivity in thin films decreases exponentially with temperature and is not temperature independent like single crystals. At its ferromagnetic transition temperature, oxygen deficient EuO undergoes a massive metal-to-insulator transition. In single crystals, its conductivity can change by more thirteen orders of magnitude. In thin-films, however, the MIT is muted and doesn't exceed 9 orders of magnitude.²⁶

Throughout the early investigation of EuO, researchers were faced with the problem of its instability in air. In 2005, Schmehl, et. al.¹⁹ demonstrated that a capping layer of amorphous silicon could protect EuO films from the oxidizing effects of standard atmospheric conditions while allowing the characterization of its structure by XRD and other property measurements to be conducted. Building upon these advances, the work reported on in this thesis demonstrates the commensurate, epitaxial growth of EuO by MBE in an adsorption-controlled regime and discusses its crystalline quality, the onset of

film relaxation of strained EuO, and its magnetic properties.

2.2 Adsorption controlled growth regime

Although the growth of epitaxial EuO films dates back over 30 years,³⁰ its formation is still a difficult balancing act between the europium and oxygen fluxes to avoid the formation of europium metal on the oxygen-poor side and Eu_3O_4 or Eu_2O_3 on the oxygen-rich side. Therefore, the traditional approach to the growth of stoichiometric EuO is to try to precisely match europium and oxygen fluxes. To avoid flux matching altogether, the use of an adsorption-controlled growth regime has been suggested³¹ and strong indications of its existence have been reported.⁸ Here we prove the existence of an adsorption-controlled growth regime for EuO and demonstrate its use. By heating the substrate to temperatures high enough to evaporate unoxidized europium metal, the deposition of EuO can be controlled solely by oxygen flux. This way, all available oxygen reacts to form EuO and the excess europium evaporates leaving pure stoichiometric EuO.

2.3 Experimental procedure

2.3.1 Seed crystal

The films were grown in a Veeco 930 MBE system (described elsewhere³²) with a base pressure less than 2×10^{-9} torr. Yttria stabilized cubic zirconia ($\text{Y}_2\text{O}_3\text{-ZrO}_2$) has an excellent lattice match to EuO, and the epitaxial growth of EuO on cubic zirconia has been demonstrated.^{8,29,33} A problem with cubic zirconia, however, is that it acts as a growth temperature-dependent oxygen source.¹⁹ We have found YAlO_3 to be free of this

problem and used single crystalline YAlO_3 substrates oriented within $\pm 0.5^\circ$ of (110) to seed the epitaxial growth of (001) EuO in this study. YAlO_3 takes the perovskite crystal structure but with distorted oxygen octahedral as seen in figure 2.1. (110) YAlO_3 has a rectilinear surface net with in-plane lattice constants of 7.431 Å along $[1\bar{1}0]$ and 7.371 Å along $[001]$.³⁴ As depicted in Fig. 2.2, EuO grows with its unit cell rotated in-plane by 45° with respect to the (110) YAlO_3 surface net. This provides a linear lattice mismatch of 2.2% for $[110] \text{EuO} \parallel [1\bar{1}0] \text{YAlO}_3$ and 1.4% for $[1\bar{1}0] \text{EuO} \parallel [001] \text{YAlO}_3$.¹⁹

2.3.2 Growth parameters

EuO films were deposited with O_2 partial pressures (P_{O_2}) ranging from 2.5×10^{-10} torr to 1×10^{-8} torr above the background pressure. The substrate temperature (T_{sub}) was approximately 590°C for all growths, significantly higher than the $T_{\text{sub}} \sim 300^\circ\text{C}$ typically used for the epitaxial growth of EuO.^{19,23,26,29} By choosing a substrate temperature comparable to the temperature of the europium source supplying the europium flux, excess europium metal is readily desorbed from the growing film. The incident europium flux was measured using a QCM, and was adjusted to 1.1×10^{14} Eu atoms/(cm²•s) for every growth. A main shutter directly in front of the substrate was opened to initiate growth only after a steady-state oxygen background partial pressure was achieved with the europium source shutter open (see figure 1.3). The growths were ended 30 min later by simultaneously closing the europium source shutter and piezoelectric oxygen valve. After allowing the substrate to cool in ultra-high vacuum, a 10 nm thick capping layer of amorphous silicon was deposited at a rate of

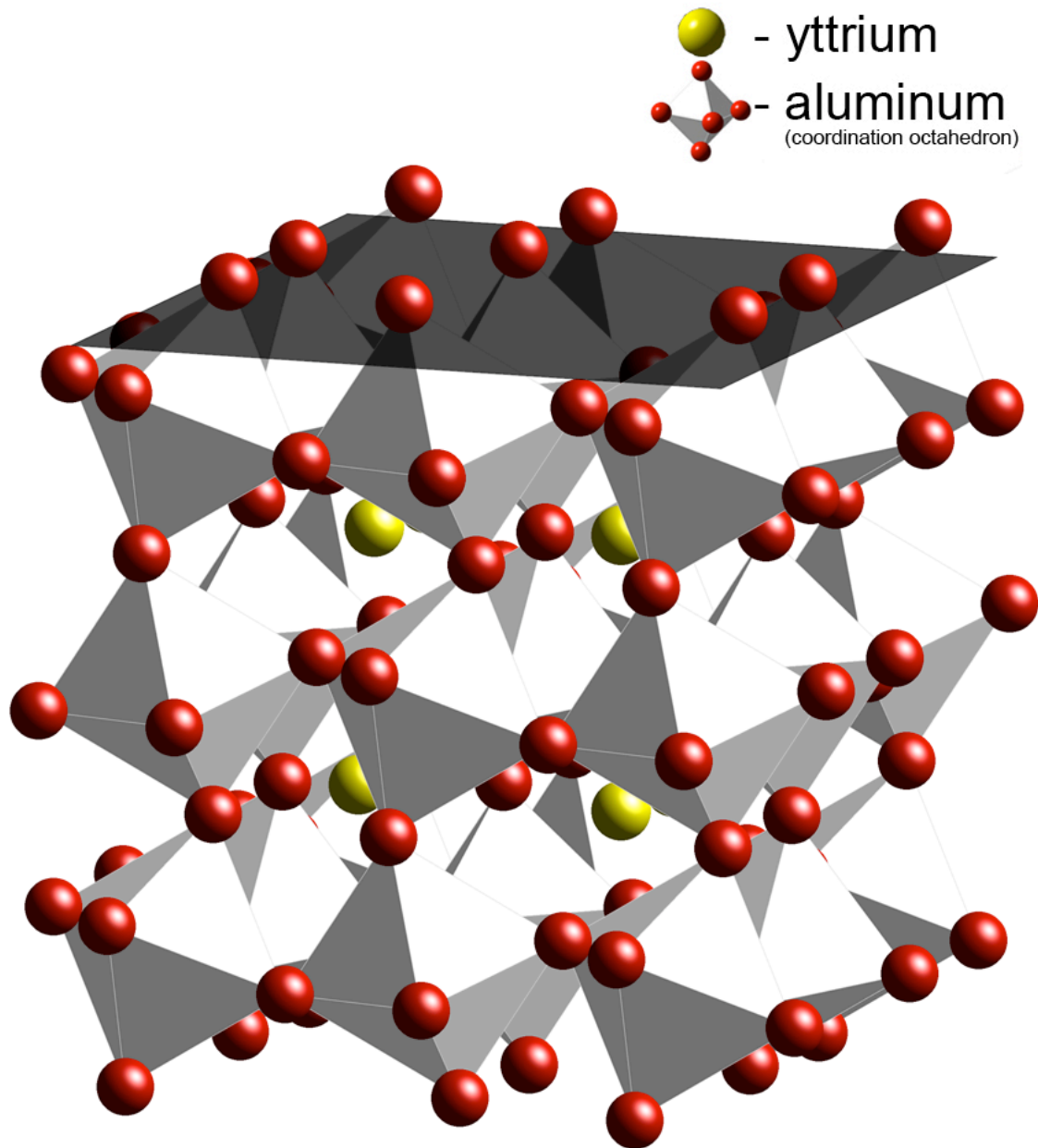


Fig. 2.1. Crystal structure of YAlO_3 with (110) surface seen in black. The octahedral oxygen cage surrounding each Aluminum atom share corners with one another as in all perovskite crystals, but are tilted with respect to one another which changes its unit cell from cubic to orthorhombic and produces a surface net upon which EuO can be grown that is rectilinear as opposed to cubic. This surface net is composed of the red oxygen atoms above the black (110) surface shown.

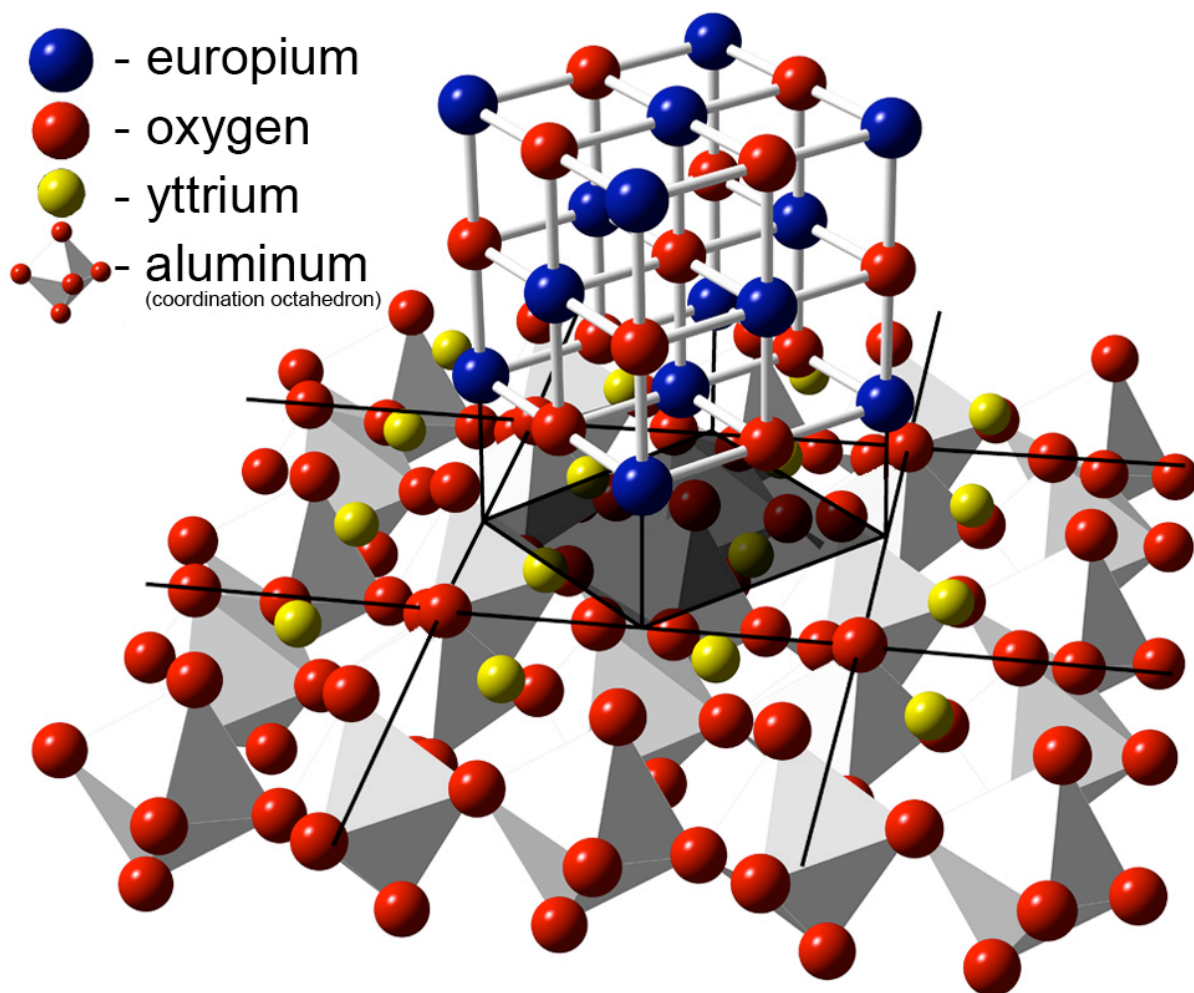


Fig. 2.2. Crystal structure of (001) EuO epitaxially grown on (110) YAlO₃ depicting the 45° rotation of the EuO unit cell (above) with respect to the pseudo-cubic YAlO₃ lattice (below).

1×10^{13} Si atoms/(cm²•s) to protect the EuO film from oxidation upon exposure to air.¹⁹

The crystal growth was monitored in situ using RHEED and ex situ using XRD.

2.4 Results and discussion

2.4.1 X-ray diffraction

Figure 2.3 shows XRD data from a 356 ± 4 Å thick (001)-oriented EuO film grown on (110) YAlO₃ at approximately 590 °C and $P_{O_2} = 1 \times 10^{-9}$ torr. The θ -2 θ XRD pattern (Fig. 2.3(a)) shows that the film is single phase. The azimuthal ϕ scan of the 111 EuO peaks (Fig. 2.3(b)) exhibits four peaks, corroborating the in-plane orientation relationship shown in Fig. 2.2 and demonstrating that the film is untwined. The in-plane lattice spacing of this EuO film was determined from the 2 θ positions of these 111 EuO peaks in combination with that of the 002 out-of plane EuO peak. Due to the distortion of the EuO film by the rectilinear surface net of the (110) YAlO₃ substrate (with dimensions 7.431 Å along $[1\bar{1}0]$ YAlO₃ and 7.371 Å along $[001]$ YAlO₃, which were confirmed by XRD on these substrates), the $[110]$ and $[1\bar{1}0]$ in-plane EuO vectors remain perpendicular, but are no longer of equal length. The measured spacing of the EuO surface net were 7.43 ± 0.068 Å along $[1\bar{1}0]$ EuO and 7.37 ± 0.068 Å along $[110]$ EuO.

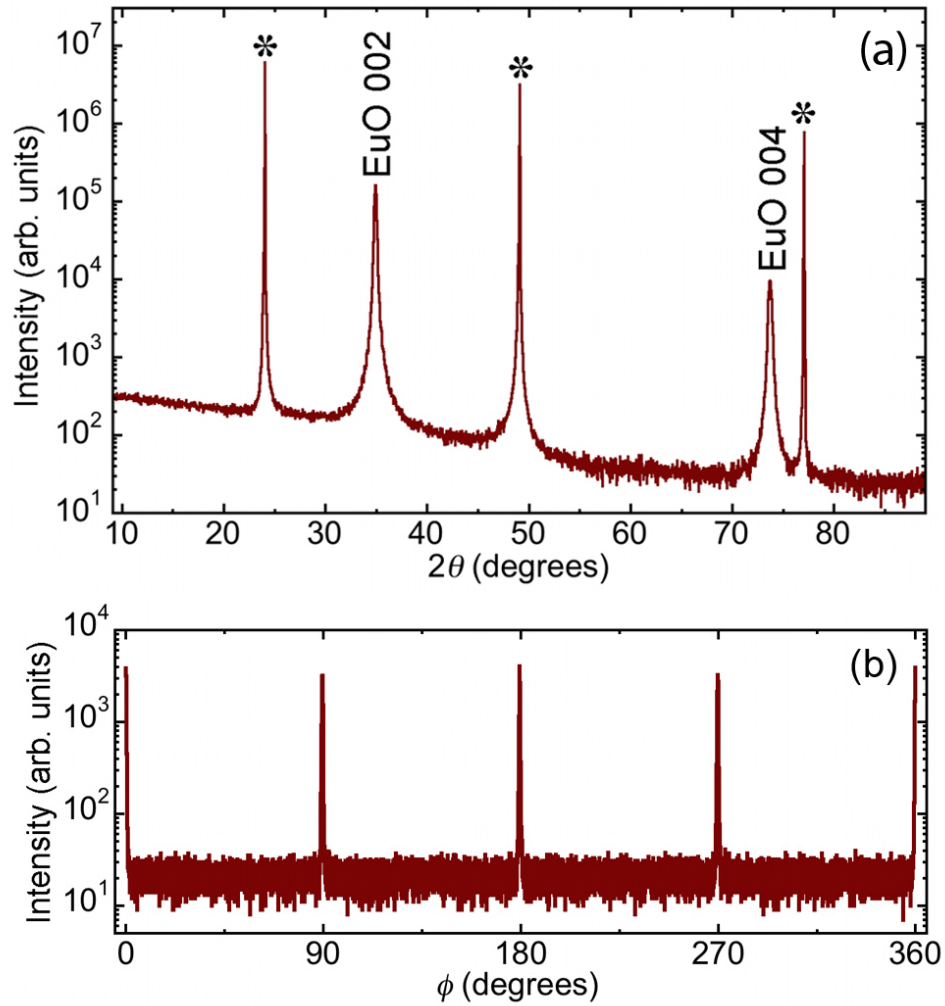


Fig. 2.3. X-ray diffraction scans from a 356 Å thick EuO film grown on (110) YAlO_3 at approximately 590 °C and 1×10^{-9} torr P_{O_2} . (a) θ - 2θ scan. (b) Azimuthal ϕ scan of the 111 EuO diffraction peaks at $\chi = 54.7^\circ$. $\chi = 0^\circ$ aligns the diffraction vector to be perpendicular to the plane of the substrate. $\phi = 0^\circ$ corresponds to the in-plane component of the diffraction vector aligned parallel to the [001] direction of the (110) YAlO_3 substrate. Together, these XRD scans show that the EuO film is epitaxial, commensurate, and oriented with $[001] \text{EuO} \parallel [110] \text{YAlO}_3$ and $[110] \text{EuO} \parallel [001] \text{YAlO}_3$.

From the XRD data in figure 2.3(a) the out-of-plane lattice spacing can be calculated with Bragg's equation:

$$n\lambda = 2d\sin(\theta)$$

In this case, $n = 2$, $\lambda = 1.5406\text{\AA}$, and $\theta = 35.110 \pm 0.150^\circ$. The out-of-plane lattice spacing (d) is therefore,

$$d = 5.119 \pm 0.057 \text{ \AA}.$$

Assuming the film lattice is coherent with that of the (110) YAlO_3 substrate, the out-of-plane lattice constant can also be calculated using the in-plane lattice constants of (110) YAlO_3 and the elastic compliance coefficients of EuO. If this value is close to the value found using XRD data it confirms that the film is indeed commensurate. In tensor notation, the relationship between stress and strain is:

$$X_{ij} = c_{ijkl} x_{kl}$$

For crystals with cubic symmetry, c_{ijkl} has only three coefficients. At 77K, these are:

$$c_{11} = 192 \text{ GPa}, c_{12} = 42 \text{ GPa}, c_{44} = 54.2 \text{ GPa}^{35}$$

To simplify the calculation, we will ignore the distortive effects of the strain anisotropy induced in EuO by (110) YAlO_3 . x_{kl} , therefore, is $(x_a, x_b, x_c, 0, 0, 0)$ in Voigt matrix notation where x_a , x_b , and x_c are the strains in the principle directions of EuO along its a , b , and c cubic axes respectively. X_a and X_b are unknown and X_c is equal to zero in this case. Assuming a full strain state, $x_a = x_b = 0.0175$. Now, using the full compliance matrix for EuO, we get:

$$\begin{bmatrix} 192 & 42 & 42 & 0 & 0 & 0 \\ 42 & 192 & 42 & 0 & 0 & 0 \\ 42 & 42 & 192 & 0 & 0 & 0 \\ 0 & 0 & 0 & 54.2 & 0 & 0 \\ 0 & 0 & 0 & 0 & 54.2 & 0 \\ 0 & 0 & 0 & 0 & 0 & 54.2 \end{bmatrix} \begin{bmatrix} 0.014 \\ 0.022 \\ x_c \\ 0 \\ 0 \\ 0 \end{bmatrix} = \begin{bmatrix} X_a \\ X_b \\ 0 \\ 0 \\ 0 \\ 0 \end{bmatrix}$$

Solve for x_c ,

$$42(0.014 + 0.022) + 192x_c = 0$$

$$x_c = -0.00766$$

Apply strain to natural lattice constant ($d' = 5.141 \text{ \AA}$),

$$d = d' (x_c)$$

$$d = 5.102 \text{ \AA}$$

This value for the out-of-plane lattice constant of strained EuO is within the error of the value obtained from XRD data above and confirms that the film is indeed coherent with the underlying (110) YAlO_3 lattice and strained in tension.

Together, these XRD results show that this EuO film is epitaxial, commensurate, and oriented with (001) EuO \parallel (110) YAlO_3 and $[110] \text{ EuO} \parallel [001] \text{ YAlO}_3$.

When integrated with (110) YAlO_3 , EuO is strained along the $[110]$ and $[1\bar{1}0]$ directions of its primitive unit cell. Because this strain is not directed along its principle crystallographic axes, its unit cell is distorted from its cubic ground state to a monoclinic structure. Figure 2.4 shows the relationship between the (110) YAlO_3 surface net and the EuO film grown upon it.

2.4.2 Reflection High-Energy Electron Diffraction (RHEED)

If the film is growing in an adsorption-controlled regime, all incident, unreacted

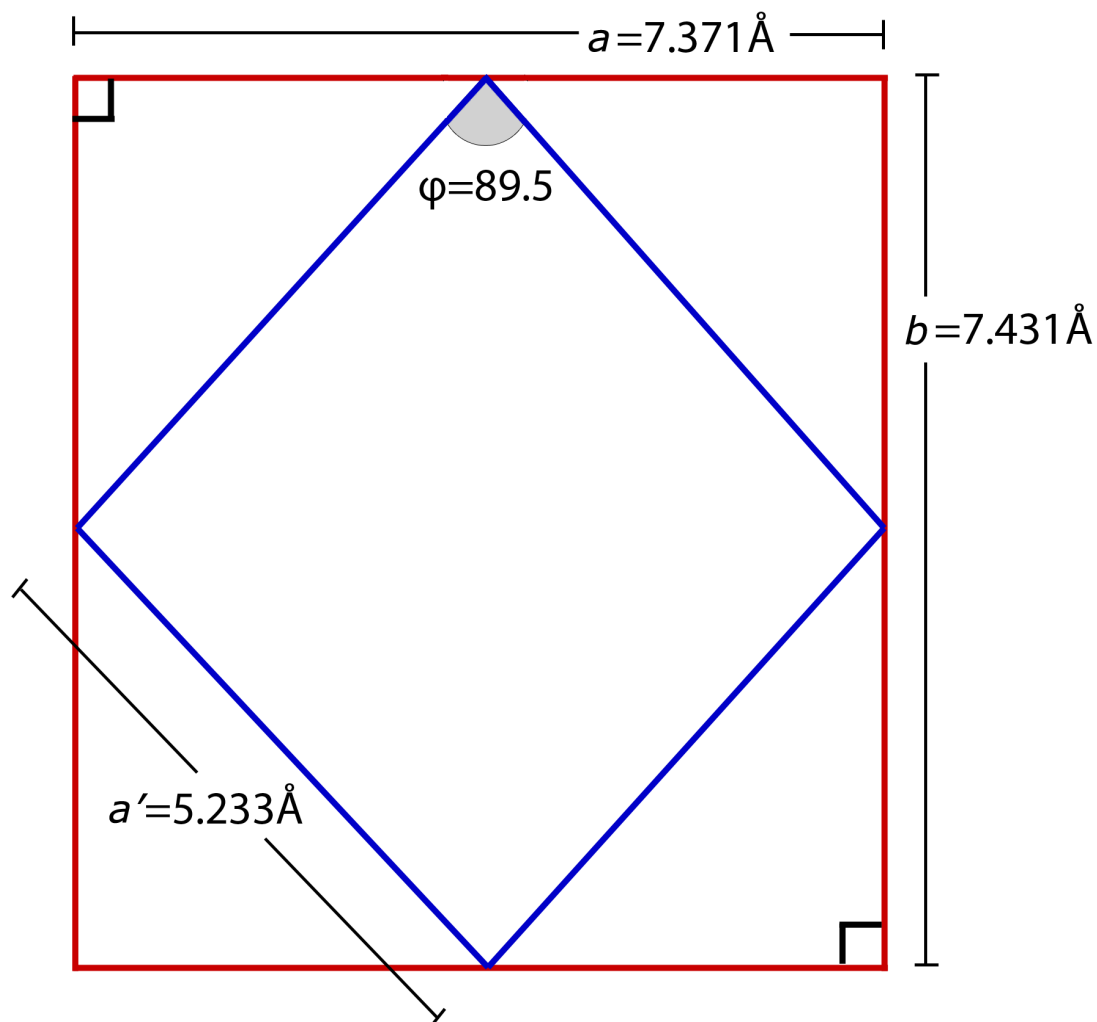


Fig 2.4. Surface net alignment of (001) EuO unit cell (in blue) on (110) YAlO₃ pseudo-cubic unit cell. The EuO thin film distorts and expands to align with the underlying (110) YAlO₃ substrate. As a result, the footprint of the EuO unit cell is no longer a square, but is a rhombus.

europium desorbs from the substrate and film surface. RHEED and XRD were used to show that in the absence of oxygen at $T_{\text{sub}} \sim 590^\circ\text{C}$ the incident europium desorbs from the substrate. RHEED imaging of a bare YAlO_3 substrate at growth temperature appeared identical before (Fig. 2.5(a)) and after (Fig. 2.5(b)) exposing it to a europium flux in the absence of oxygen. The sample was capped with silicon and the absence of a europium metal film was confirmed by XRD. Figure 2.5 depicts RHEED imagery of (110) YAlO_3 before and after exposure to europium flux and after exposure to simultaneous europium and oxygen flux.

2.4.3 Oxygen flux dependence

EuO films were grown in differing background partial pressures of oxygen and their europium content was determined using RBS. Using the density of crystalline EuO , this RBS atomic coverage was converted to film thickness. As shown in Fig. 2.6, as the P_{O_2} used during growth increases, so does the film thickness, indicating a faster growth rate. The observed dependence of film thickness on the oxygen partial pressure (oxygen flux) is a hallmark of adsorption-controlled growth. For films grown with P_{O_2} higher than 2×10^{-9} torr, where the oxygen flux becomes greater than the europium flux, the growth rate saturates, and higher oxidation states such as Eu_3O_4 begin to form.

2.4.4 Strain relaxation

Rocking curves from the 002 EuO peaks of films with different thicknesses and the 220 peak of a YAlO_3 substrate are shown in Fig. 2.7. Rocking curves were obtained with ϕ aligned such that the in-plane component of the diffraction vector is parallel to one

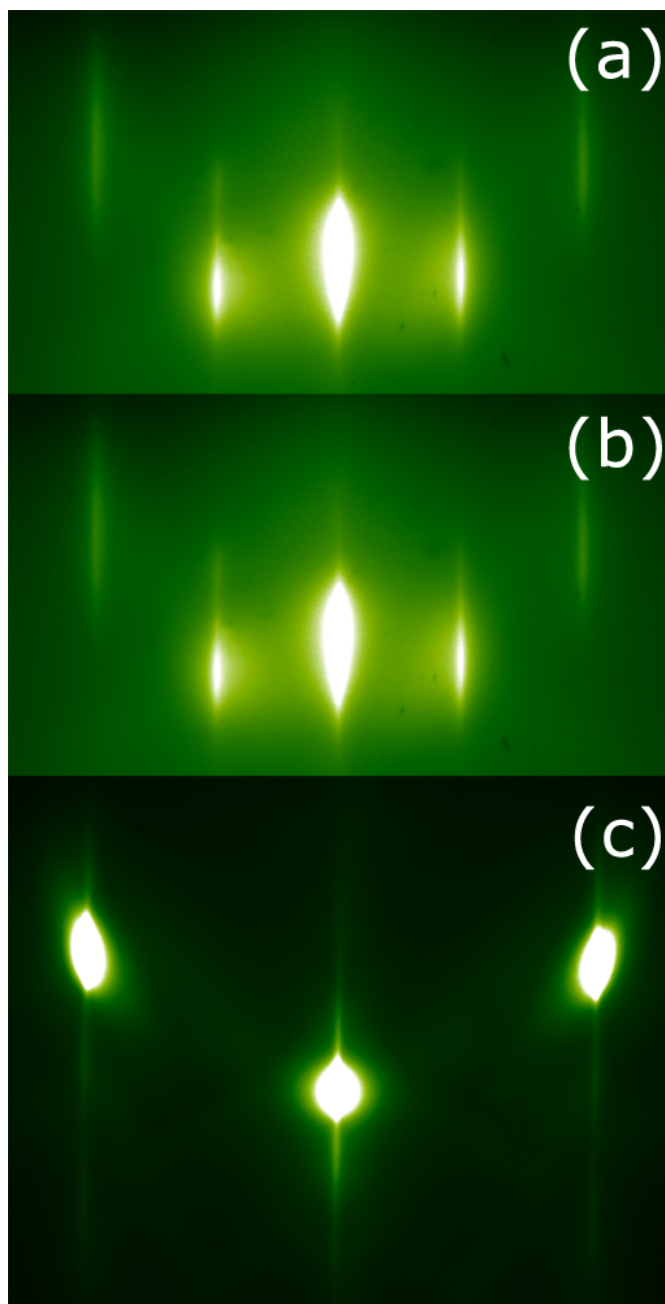


Fig. 2.5. Reflection high-energy electron diffraction (RHEED) patterns of (110) YAlO_3 along its [001] azimuth (a) before and (b) after exposure to europium flux at 590°C (above the minimum adsorption controlled growth temperature). (c) RHEED pattern of (001) EuO along its [110] azimuth as grown on (110) YAlO_3 under adsorption-controlled conditions.

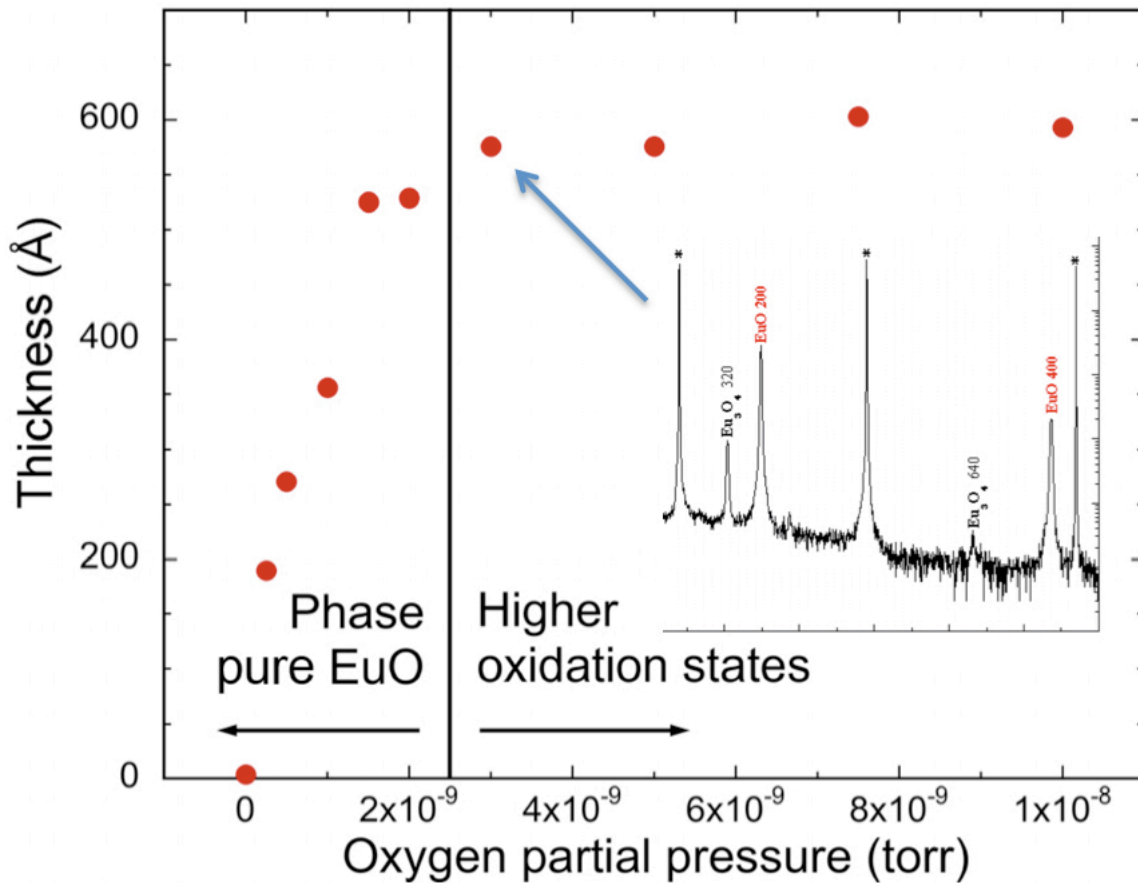


Fig. 2.6. Film thickness (determined by RBS) as a function of the oxygen background partial pressure (P_{O_2}) used during the growth. Each film was grown at approximately 590 °C for 30 minutes in the adsorption-controlled regime with a europium flux of 1.1×10^{14} Eu atoms/(cm²•s). Below roughly 2.5×10^{-9} torr, the EuO films remain phase pure and additional oxygen reacts with excess europium, increasing the growth rate. At roughly 2.5×10^{-9} torr, the europium and oxygen fluxes are matched and increasing P_{O_2} results in the formation of impurity phases (first Eu₃O₄ and then Eu₂O₃) containing higher oxidation states of europium. Inset displays Eu₃O₄ impurity peaks in XRD scan.

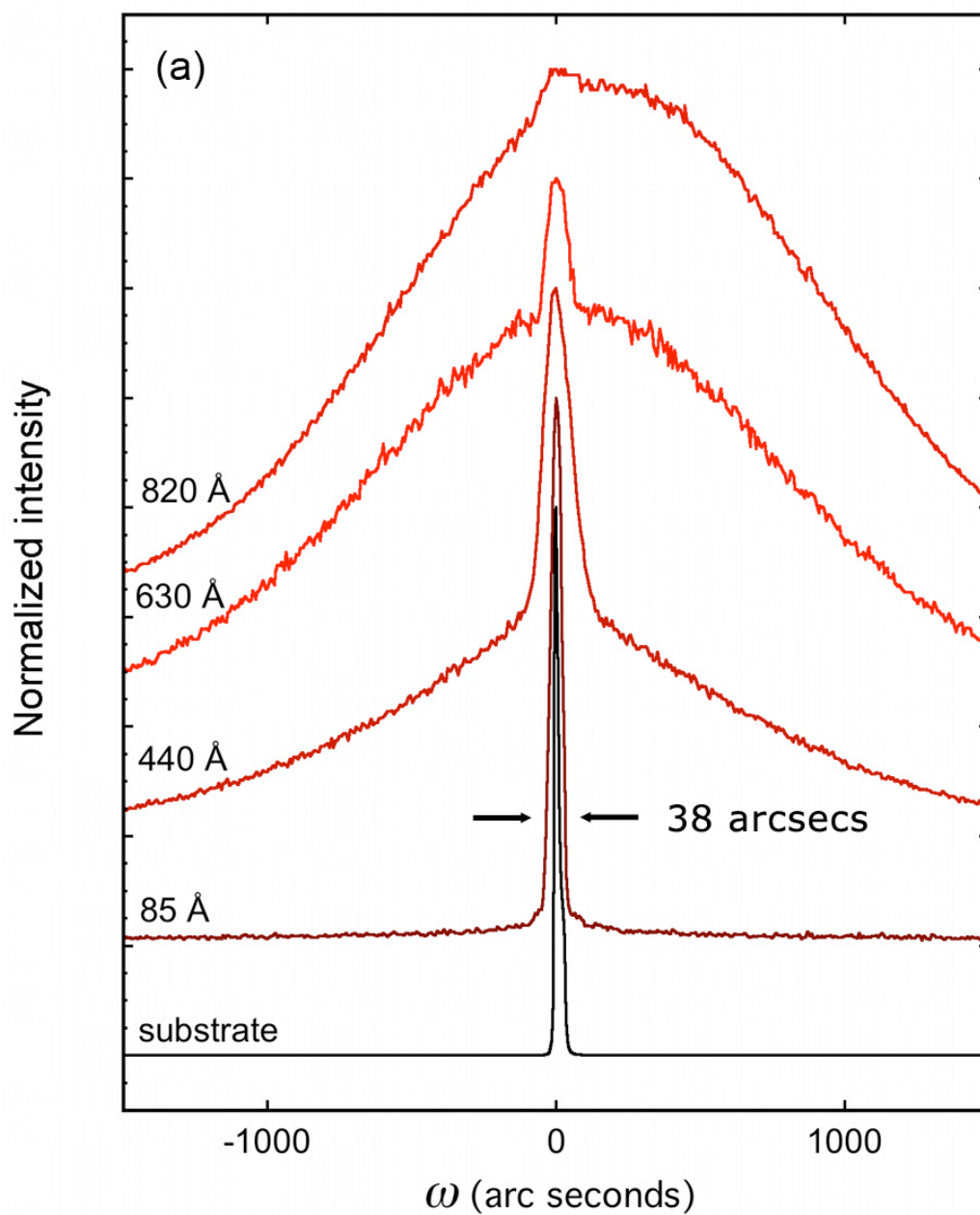


Fig. 2.7. Rocking curves from the 002 EuO peaks of films with different thicknesses and the 220 peak of a YAlO_3 substrate. Two superimposed peak shapes near 440 Å indicate film relaxation through misfit dislocations. The peak intensities are normalized and shifted relative to one another for clarity.

of the four $\langle 100 \rangle$ -type EuO in-plane directions that are equally strained. Films grown thinner than the thickness at which relaxation begins under these growth conditions display sharp rocking curves with full width at half maximum (FWHM) as narrow as 34 arc sec, comparable to those of the substrates (12-34 arc sec). Partially relaxed films show the same sharp peaks on top of a broad background peak originating from the relaxed portion of the film. As the films grow beyond the onset of relaxation, the intensity of the broad background peak increases as defects are formed and the intensity of the sharp central peak decreases as less and less of the film is commensurately strained. The broad background peak also shifts to higher values of theta indicating an expansion of the out of plane lattice constant during relaxation.

As discussed previously, the EuO in-plane lattice spacings of a 356 ± 4 Å thick film closely matched those of the (110) YAlO_3 . In contrast, the in-plane spacings of an 820 ± 8 Å thick EuO film were determined to be 7.28 ± 0.027 Å along $[1\bar{1}0]$ EuO and 7.28 ± 0.027 Å along $[110]$ EuO. The out-of-plane lattice spacing was 5.14 Å. Figure 2.8 shows the rocking curve FWHM of the 002 EuO film peak as a function of film thickness d . For d less than 356 ± 4 Å, the films maintain a narrow rocking curve. For d greater than 440 ± 4 Å, the rocking curve FWHM begins to broaden in a manner consistent with other epitaxial semiconductor and oxide films undergoing relaxation.³⁶⁻³⁸ From $d = 820 \pm 8$ Å and beyond, no commensurate central peak is observed in the rocking curves. The onset of film relaxation agrees well with the onset of broadening of the FWHM of the rocking curves.

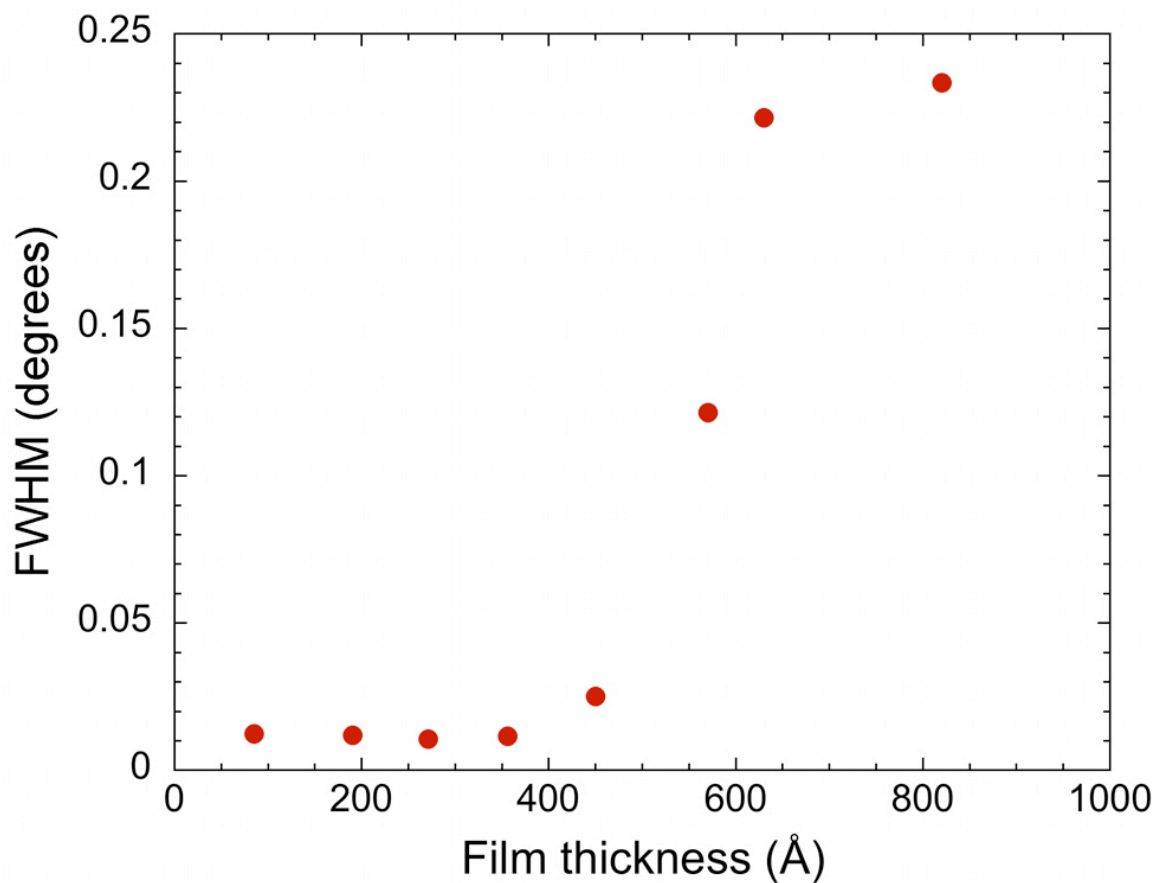


Fig. 2.8 FWHM of the 002 EuO film peak as a function of the film thickness. Narrow FWHMs comparable to that of the 220 peak of the YAlO_3 substrates are maintained for EuO film thicknesses below ~ 380 Å. The FWHM begins to broaden beyond this thickness.

2.4.5 Magnetic properties

The magnetic properties of a coherently strained EuO film were measured by Andreas Schmehl using a superconducting quantum interference device (SQUID). As seen in figure 2.9, the ferromagnetism sets in at 69 K when cooled without an external magnetic field and grows to $6.96 \pm 0.07 \mu_B$ per Eu atom under a saturating external magnetic field at 5 K, 99.5% of its theoretical maximum (figure 2.10). This is consistent with single crystalline EuO (Ref. 9) and is the highest reported saturated magnetization for a thin film of EuO.

2.5 Conclusions

In summary, we have established that epitaxial EuO films can be grown in an adsorption-controlled growth regime by MBE on (110) YAlO₃ and determined the critical thickness for the coherent, epitaxial growth of such films. These films exhibit rocking curve FWHMs approaching those of the YAlO₃ substrates on which they are grown. High quality films such as these minimize the extrinsic effects arising from defects in the crystal and will allow for the fundamental properties of EuO (e.g., the dependence of T_c on strain³⁹) to be established.

The next major hurdle for development of EuO in spintronic devices is overcoming the low 69 K ferromagnetic transition temperature. Therefore, future work includes growing EuO coherently on various substrates that induce a range of strain states from compressive to tensile. As predicted, compressive strain should boost T_c by as much as 30%³⁹ and demonstration of this effect will be a big step forward in the development of EuO. Unfortunately there are very few commercially available substrates

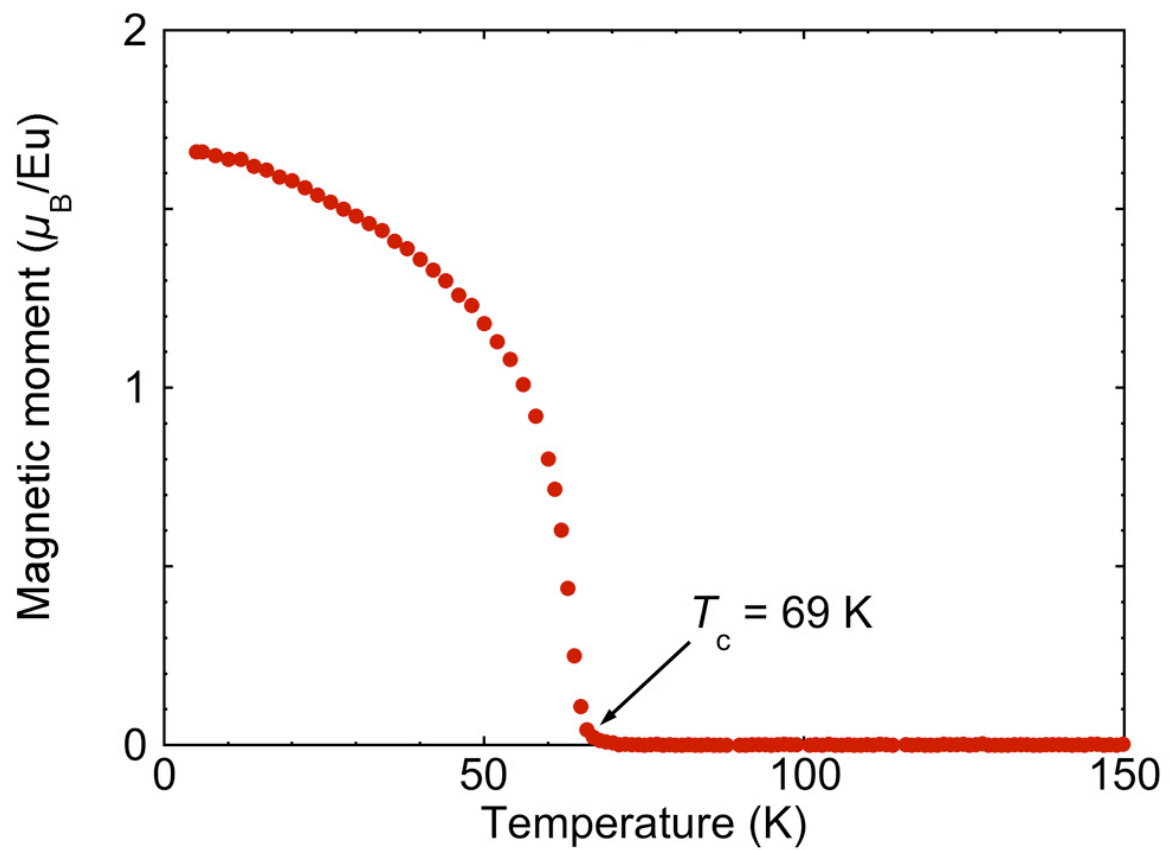


Fig. 2.9. Zero-field temperature dependence of the magnetic moment of a 271 ± 3 Å thick, commensurately strained EuO film grown on (110) YAlO_3 . The onset of ferromagnetism occurs at 69 K.

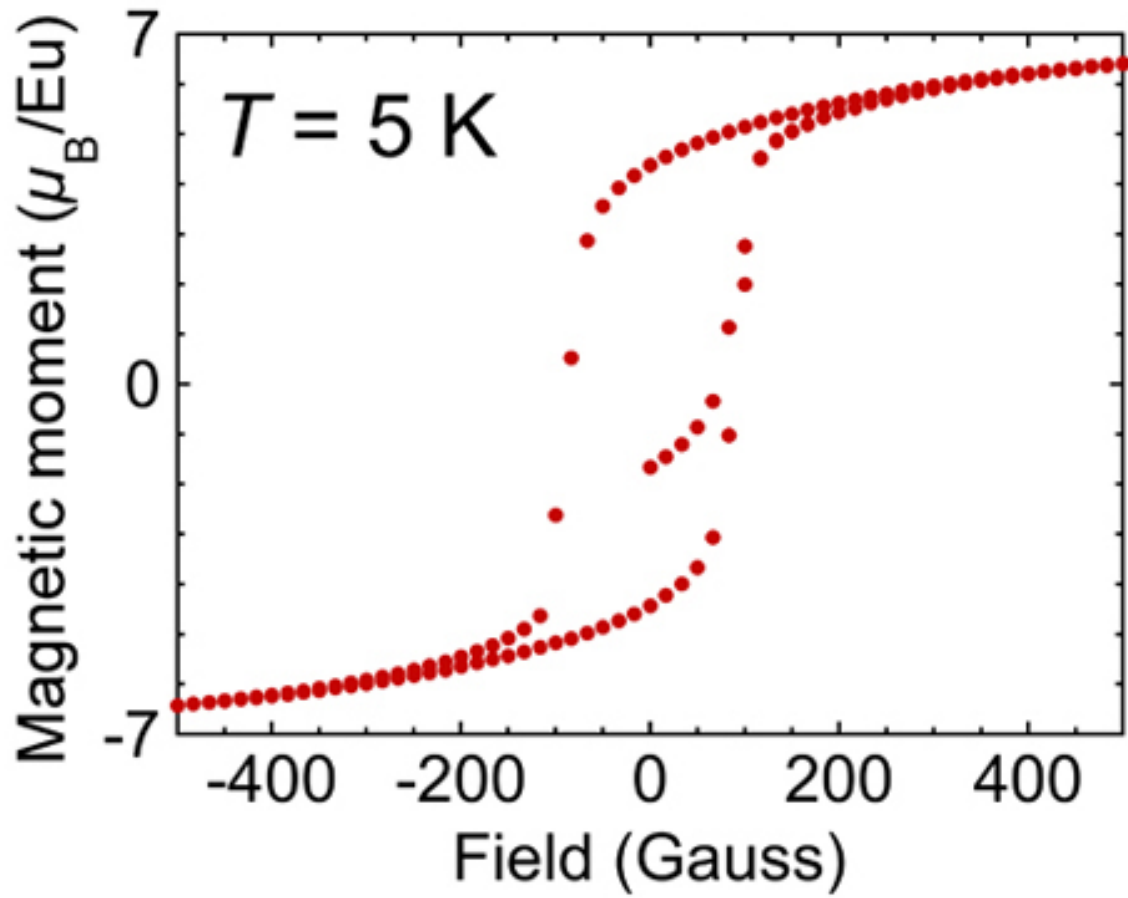


Fig 2.10. At 5 K, the magnetic hysteresis shows ferromagnetic behavior with a saturation magnetization of $6.96 \pm 0.07 \mu_B$ per europium atom, 99.5% of its theoretical maximum.

that have appropriate lattice matching to induce compressive strain in EuO without being so mismatched that coherent growth is impossible. One possible candidate is carbon in the cubic diamond crystal structure, which would induce a compressive strain of roughly -2%. Carbon however is not an ideal substrate material and it is unclear just how it will react with EuO. It may even react with the low background oxygen partial pressure during EuO growth. The $(1\bar{1}02)$ surface of corundum (Al_2O_3) will produce a strain state of roughly -4%, but this crystal system is hexagonal and the $(1\bar{1}02)$ surface net is rectilinear producing large strain anisotropies.

Future studies in doping EuO will also be of critical importance to boosting T_c and making EuO a viable material for real world applications. Doping with such ions as Gd^{3+} have been shown to boost T_c in thin films up to 170 K²³ and if the same effect can be demonstrated in commensurate epitaxial thin films, then the effect of strain and doping can possibly be combined to boost the ferromagnetic transition temperature of EuO to as high as 220 K.

Chapter 3: Alternative substrates

3.1 Introduction

Using the adsorption controlled technique described in chapter 2, EuO has been epitaxially integrated with several new substrates in addition to (110) YAlO_3 , including (001) LaAlO_3 , (001) YSZ with a 100 nm thick SrO oxygen buffer layer to block oxygen diffusion from the YSZ substrate into the EuO film, (1 $\bar{1}$ 02) Al_2O_3 , and (001) Diamond. Table 3.1 summarizes the growth conditions used to produce these films as well as the final film thickness and whether it grew coherently or not.

3.2 Lanthanum Aluminate

Above 800 K, LaAlO_3 has a cubic perovskite crystal structure as can be seen in figure 3.1. The lattice mismatch between (001) EuO and (100) LaAlO_3 induces a 4% tensile strain in EuO. According to Ref. 39 this should reduce the Curie temperature of EuO. A commensurate EuO film was successfully grown on (100) LaAlO_3 and T_c was indeed reduced from 69 K to 40 K thus adding validity to this prediction (see fig. 3.2). Because of the large lattice mismatch between (001) EuO and (100) LaAlO_3 , the EuO film cannot be grown thicker than ~ 20 Å without relaxing to its natural lattice spacing. At this thickness, no peak can be observed with XRD, but a change in the RHEED pattern can be detected. Figure 3.3 (a) shows the RHEED pattern from the (100) LaAlO_3 substrate and 3.3 (b) shows the RHEED pattern from the 16 Å thick (001) EuO film. 3.3 (c) is the RHEED pattern of a (001) oriented EuO film on (100) LaAlO_3 that grew

substrate	T_{sub}	P_{O_2} (torr)	Eu flux ($\text{at}/\text{cm}^2/\text{s}$)	film thickness (nm)	coherent? [†]
(110) YAlO_3	590 °C	1×10^{-9}	1.14×10^{14}	25	yes
(100) LaAlO_3	590 °C	1×10^{-9}	1.14×10^{14}	1.6	yes
(001) YSZ^\ddagger	590 °C	1×10^{-9}	1.14×10^{14}	100	yes
(1 $\bar{1}$ 02) Al_2O_3	682 °C	1×10^{-9}	1.14×10^{14}	53.4	no
(100) diamond	709 °C	1×10^{-9}	1.14×10^{14}	100	no

Table 3.1. Substrates, growth conditions, and film properties for all substrates used to grow (001) oriented epitaxial EuO with the adsorption-controlled method.

[†]A film is coherent if its in-plane lattice constants match those of the substrate it was grown on either because it is biaxially strained or because the natural lattice constants of both substrate and film are equal as is the case with (001) YSZ.

[‡]Ytria stabilized zirconia (YSZ) is ZrO_2 with enough yttrium substituted into the zirconium sublattice to stabilize the crystal structure in cubic symmetry.

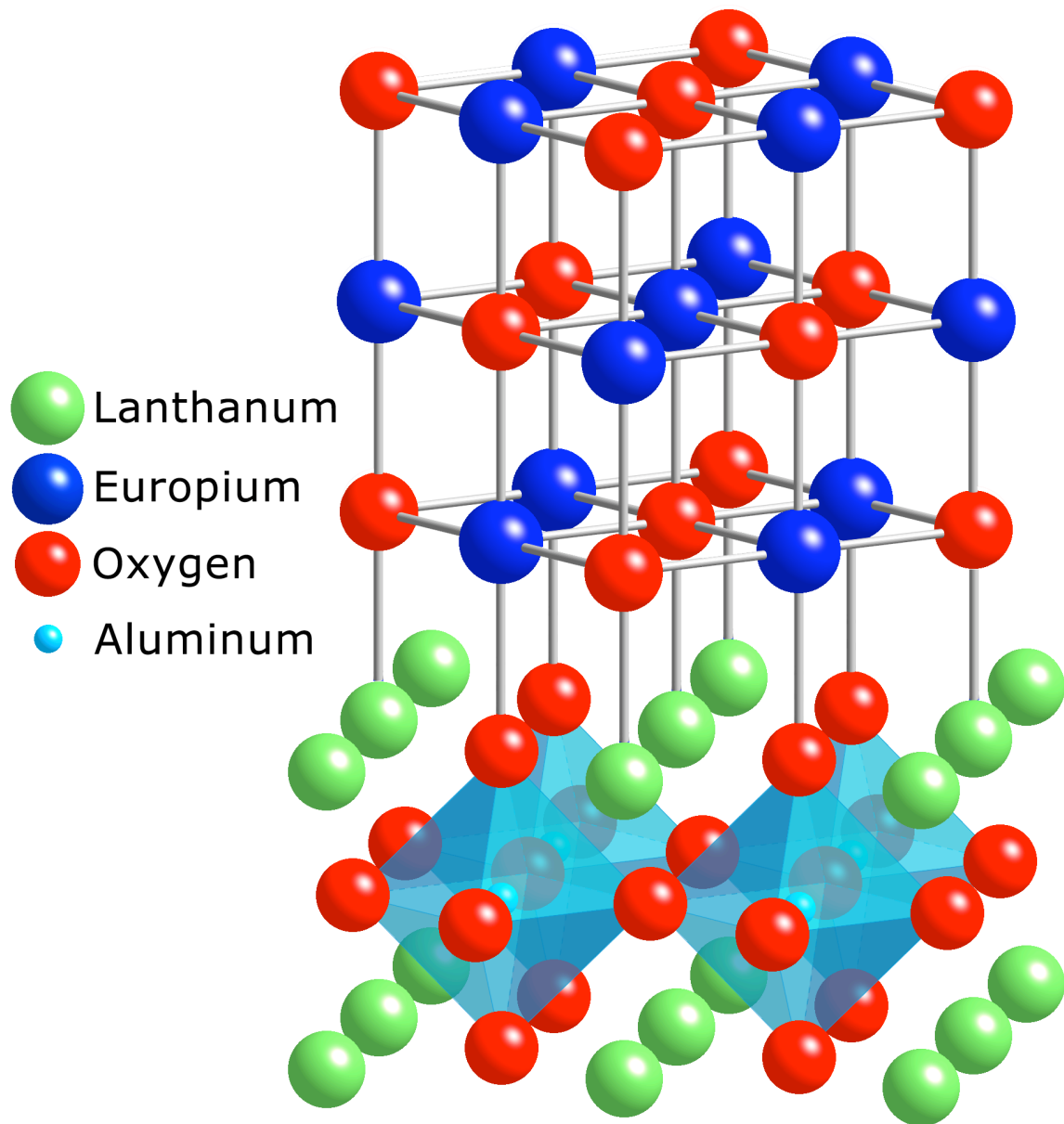


Figure 3.1. Epitaxial alignment of (001) EuO on cubic (100) LaAlO_3 (relevant at the temperature at which EuO is epitaxially grown). The oxygen octahedra surrounding each titanium atom in LaAlO_3 is shown in light blue.

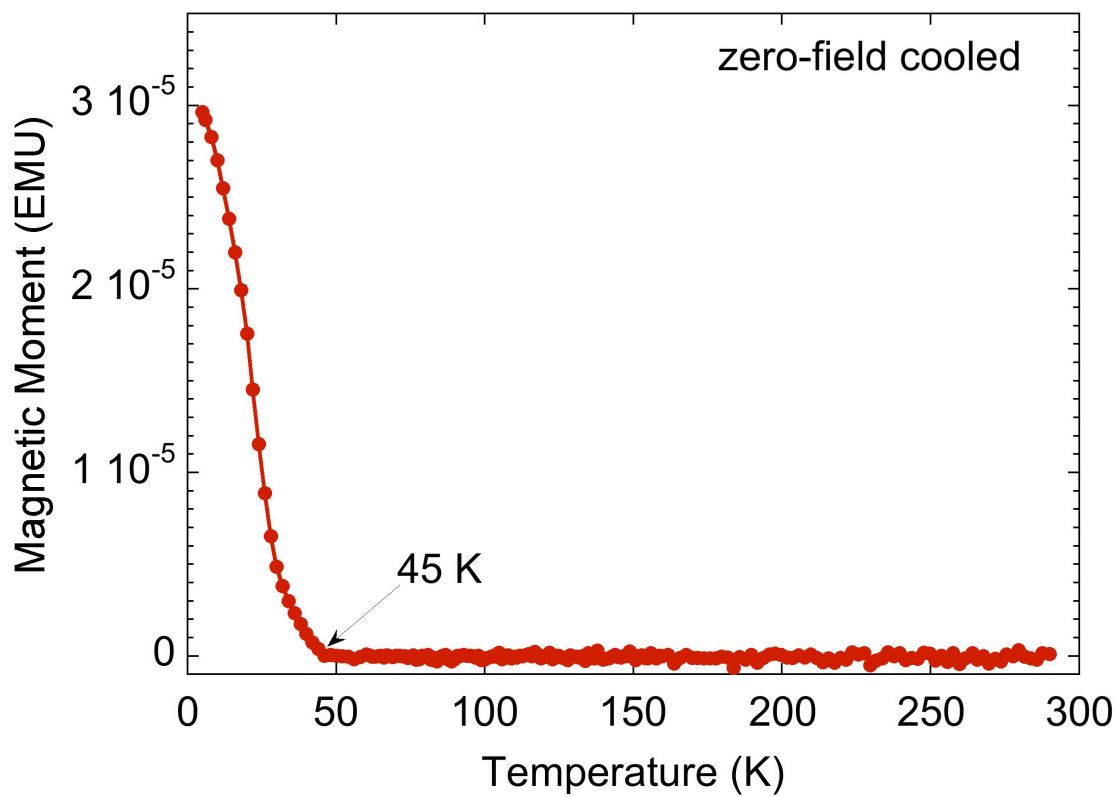


Figure 3.2. Magnetization versus temperature for EuO strained in tension on (100) LaAlO_3 . As predicted in ref. 39 the ferromagnetic transition temperature was reduced from 69 K found in unstrained samples to 45 K.

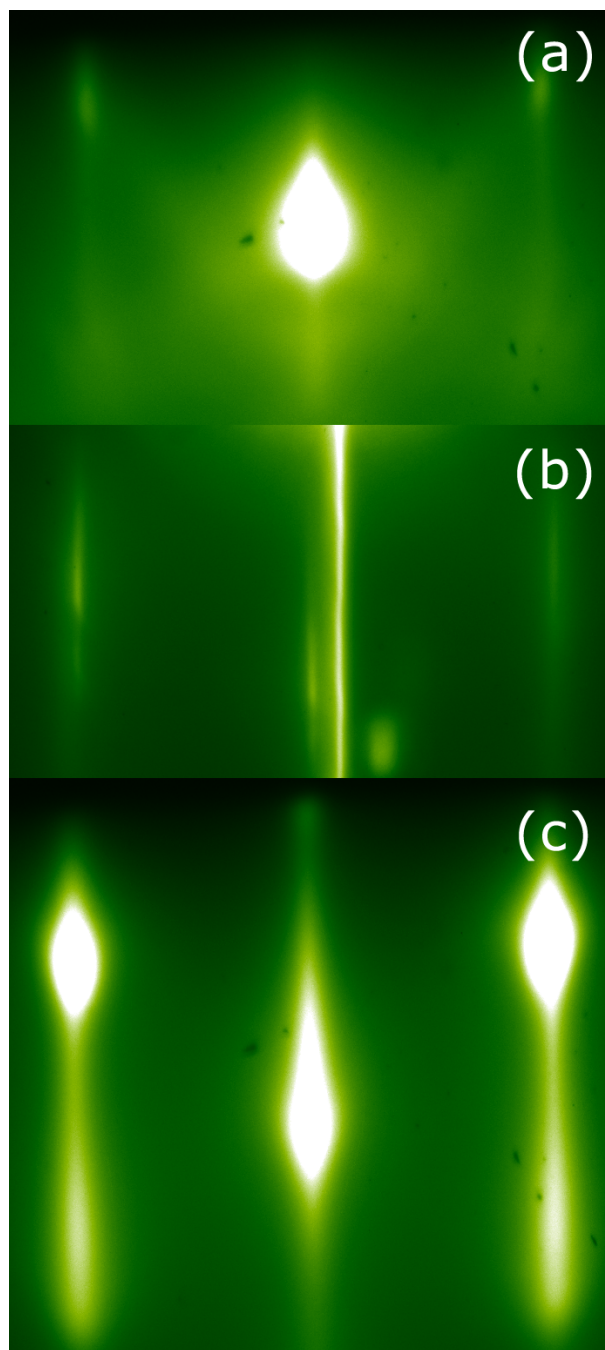


Figure 3.3. RHEED patterns of (a) a bare (100) LaAlO_3 substrate, (b) a coherent (001) EuO film (16 Å) grown on top, and (c) a relaxed (001) EuO film (60 Å) grown on a different (100) LaAlO_3 substrate .

Note: the streak seen in 3.3 (b) is due to an imaging error and is not representative of the crystal structure.

beyond its relaxation thickness. Because of imperceptible signal in XRD, this, along with the observed reduction in T_c is the only evidence that the film is strained. To further confirm this the XRD patterns of the crystal can be observed using high-intensity, synchrotron radiation.

3.3 Yttria Stabilized Zirconia

YSZ takes the fluorite crystal structure with a lattice constant of 5.14 Å, as seen in figure 3.4. Between (001) oriented YSZ and (001) EuO there exists a negligible lattice mismatch of only 0.04%. This would, all else being equal, make it an ideal substrate for the epitaxial growth of EuO. However, YSZ acts as an oxygen donor for EuO and when EuO is grown directly on top of it, phases of Eu_3O_4 and Eu_2O_3 form. In order to protect the EuO film from over oxidation by YSZ but without losing their ideal lattice match, a 100 nm (001) SrO buffer layer was grown on (001) YSZ before growing (001) EuO. SrO also has the same cubic lattice spacing as EuO and YSZ and thus very thick films of commensurate and high quality EuO can be grown in this configuration. The $\theta - 2\theta$ of such a crystal is shown in figure 3.5. Because the out-of-plan lattice constants of (001) YSZ, (001) SrO, and (001) EuO are all roughly 5.14 Å, the corresponding peaks in $\theta - 2\theta$ overlap and only one set of peaks is seen. Figure 3.6 shows the RHEED patterns produced by the YSZ substrate and both the SrO and EuO layers.

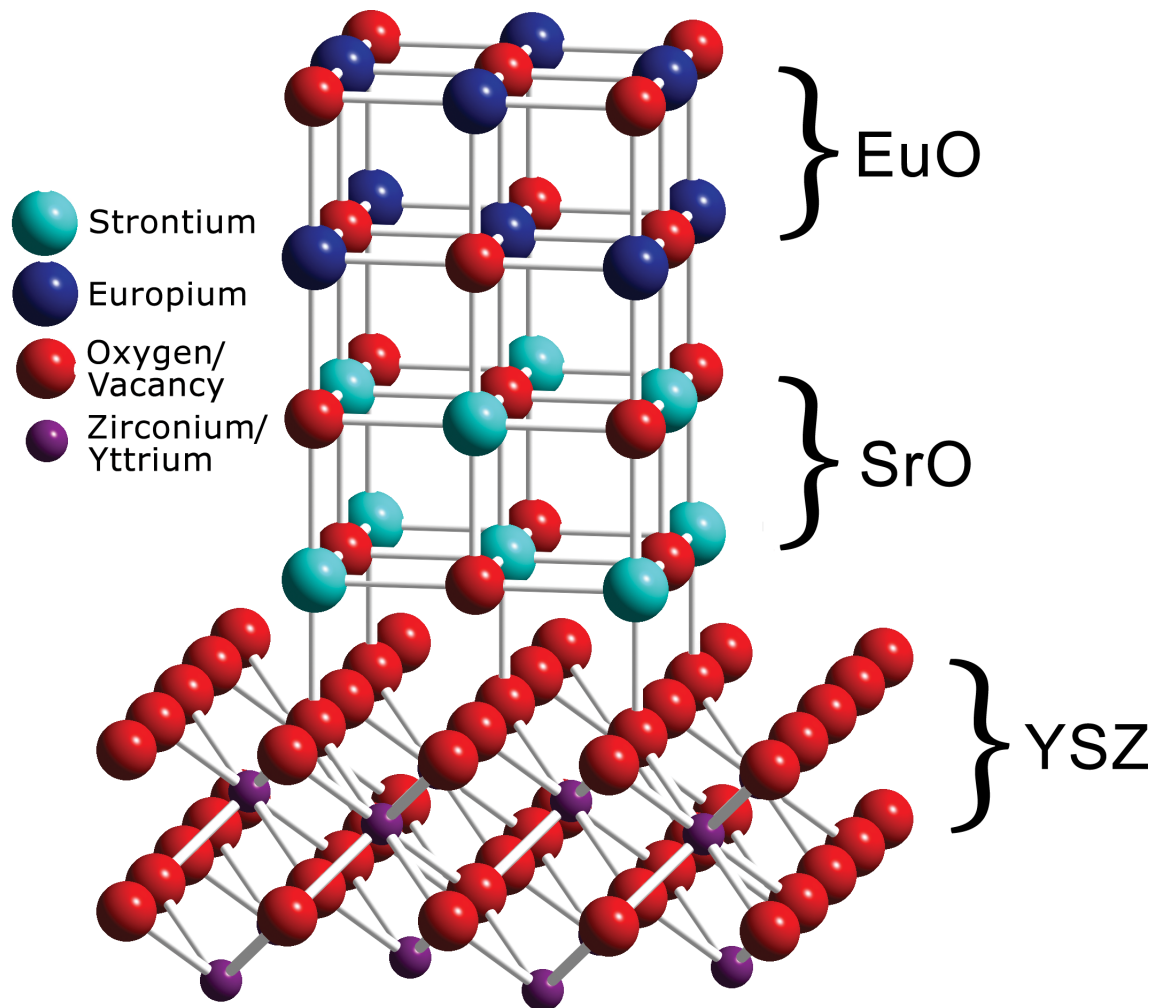


Figure 3.4. Schematic of (001) YSZ // (001) SrO // (001) EuO. While zirconia is naturally monoclinic, when appropriately doped with yttrium, it is stabilized in the cubic phase. The charge discrepancy between zirconium and yttrium causes oxygen vacancies to form. Two sublattices are thus present in the substrate. One of zirconium doped with yttrium and one with oxygen doped with oxygen vacancies. In actual films the SrO layer is 100 nm thick and is shown here as two monolayers for demonstration only.

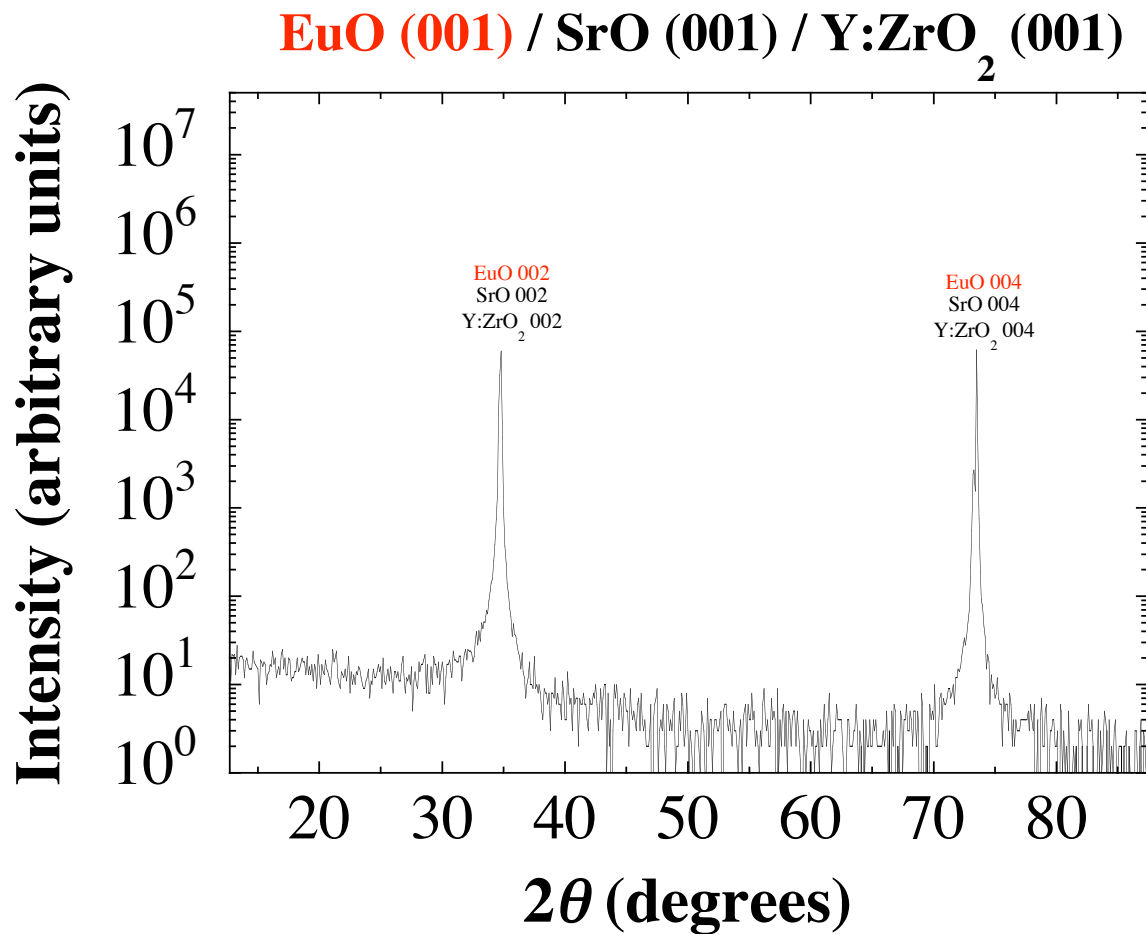


Figure 3.5. θ - 2θ XRD scan of a (001) YSZ // (001) SrO // (001) EuO crystal. Because the out-of-plan lattice constants of (001) YSZ, (001) SrO, and (001) EuO are all roughly 5.14 Å, the corresponding peaks in θ - 2θ overlap and only one set of peaks is seen.

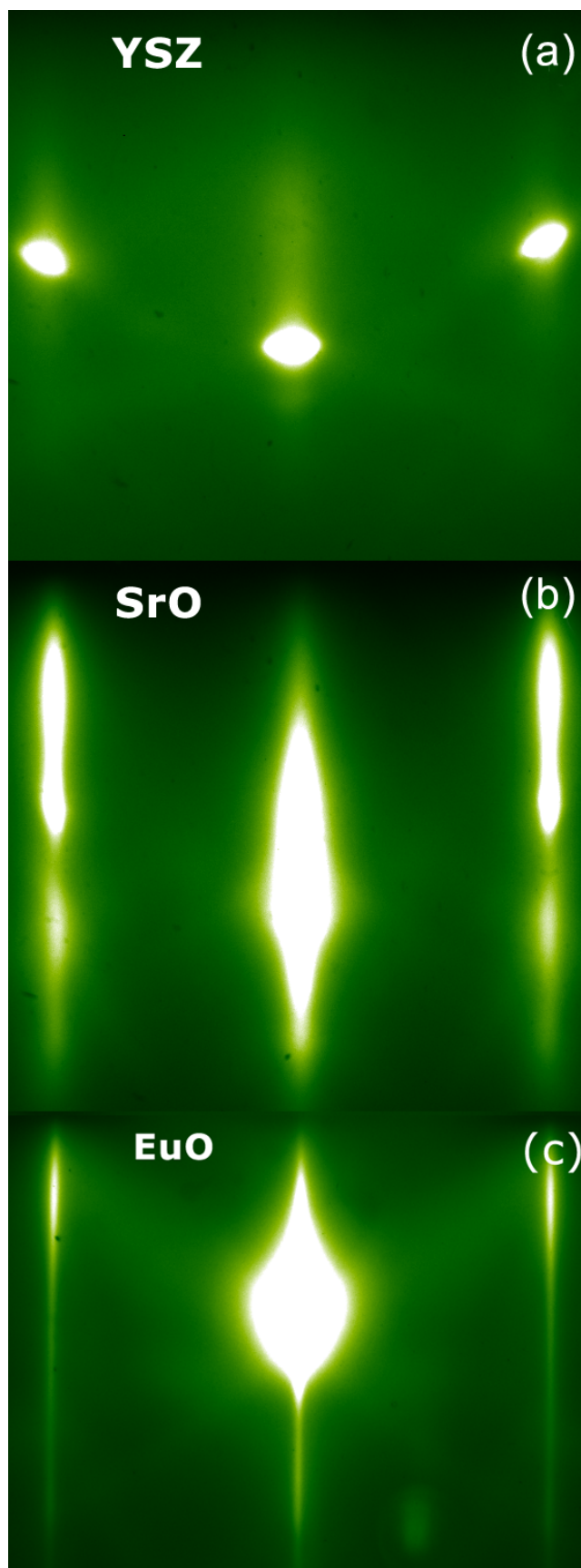


Figure 3.6. RHEED patterns produced by (a) (001) YSZ, (b) (001) SrO, and (c) EuO.

3.4 Sapphire

(1 $\bar{1}02$) Al_2O_3 has a hexagonal crystal structure. Its (1 $\bar{1}02$) surface presents a rectilinear surface net with an areal mismatch to EuO of roughly -4%. Because of the discrepancy in crystal structure types and lattice net shapes, strained growth of EuO on (1 $\bar{1}02$) Al_2O_3 was not achieved, though it did grow epitaxially in the (001) direction out-of-plane and with (100) EuO and (010) EuO oriented parallel to the surface net of (1 $\bar{1}02$) Al_2O_3 seen in figure 3.7. Figure 3.8 shows the RHEED pattern of the bare (1 $\bar{1}02$) Al_2O_3 substrate (3.8(a)) and the epitaxial EuO film (3.8(b)). Both images were captured without altering the sample orientation relative to the RHEED beam. Figure 3.9 is the 2θ XRD pattern of the same sample taken after it was capped with silicon and removed from the MBE chamber. If strained EuO can be grown on (1 $\bar{1}02$) Al_2O_3 , the high compressive strain could induce a large boost in the ferromagnetic transition temperature of EuO.

3.5 Diamond substrate

In recent years, diamond has emerged as a promising material for spintronic applications with advances in fabrication and doping of single crystalline thin films.^{40,41,42,43,44} Though it is an insulator when undoped with a band gap of 5.5 eV, diamond becomes a semiconductor when appropriately doped. This allows electrons at impurity centers to be polarized by light at optical wavelengths. The dopant of choice is nitrogen, which typically forms a nitrogen-vacancy (N-V) pair in the solid but acts as a single impurity for all intents and purposes. With diamond doped in this way, spin

lifetimes can be as high as 1 ms at room temperature⁴³ which is more than enough to carry out many tasks envisioned for this material without the need for extensive cooling.

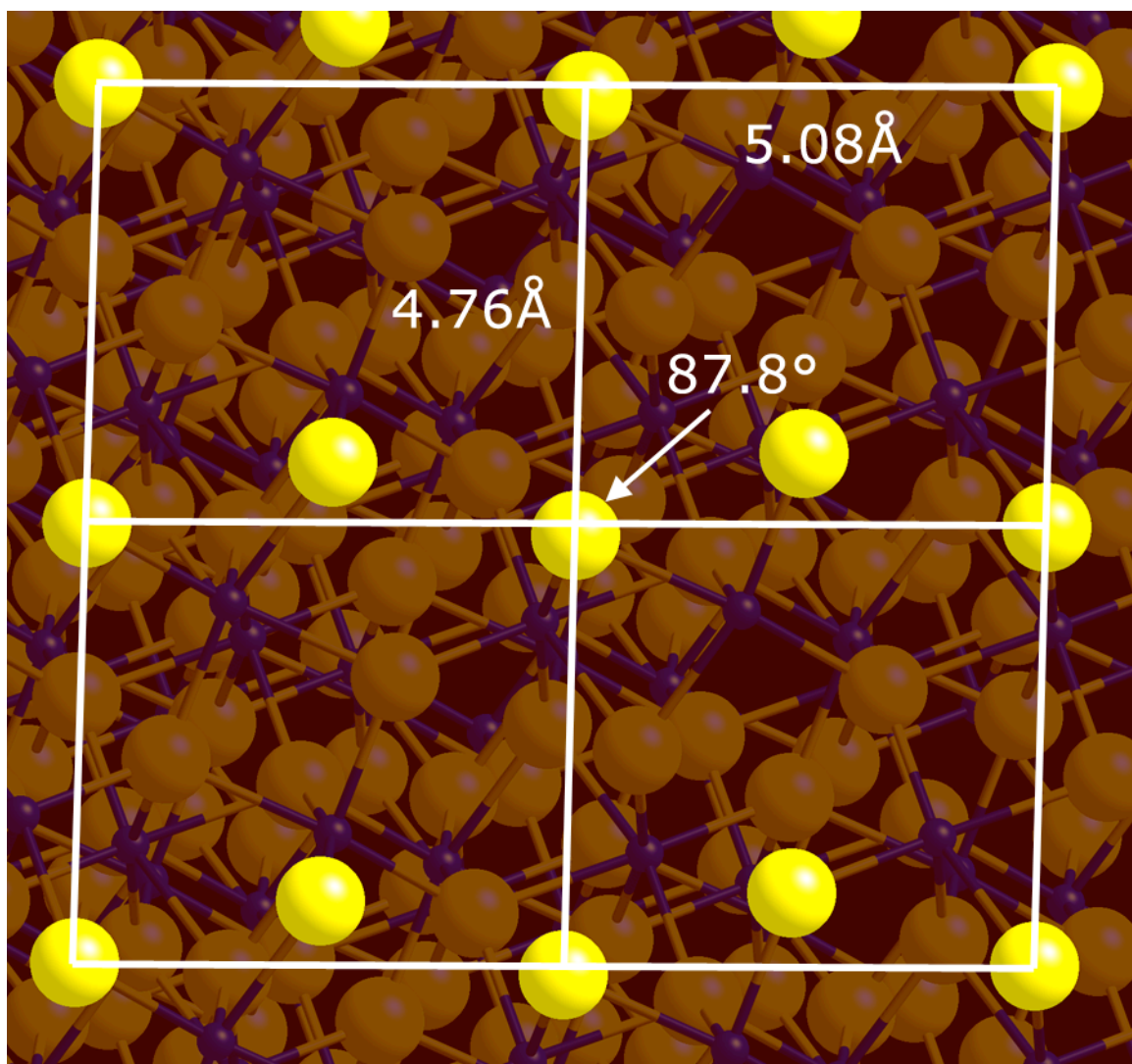


Figure 3.7. The $(1\bar{1}02)$ surface of Al_2O_3 . The oxygen atoms on the surface (seen in yellow) form a rectilinear surface net from which EuO can grow epitaxially with the principle axes of its unit cell oriented parallel to the principle axes of the surface net. If EuO grew coherently upon $(1\bar{1}02)$ Al_2O_3 a biaxial strain of $\sim 4\%$ would be induced in it.

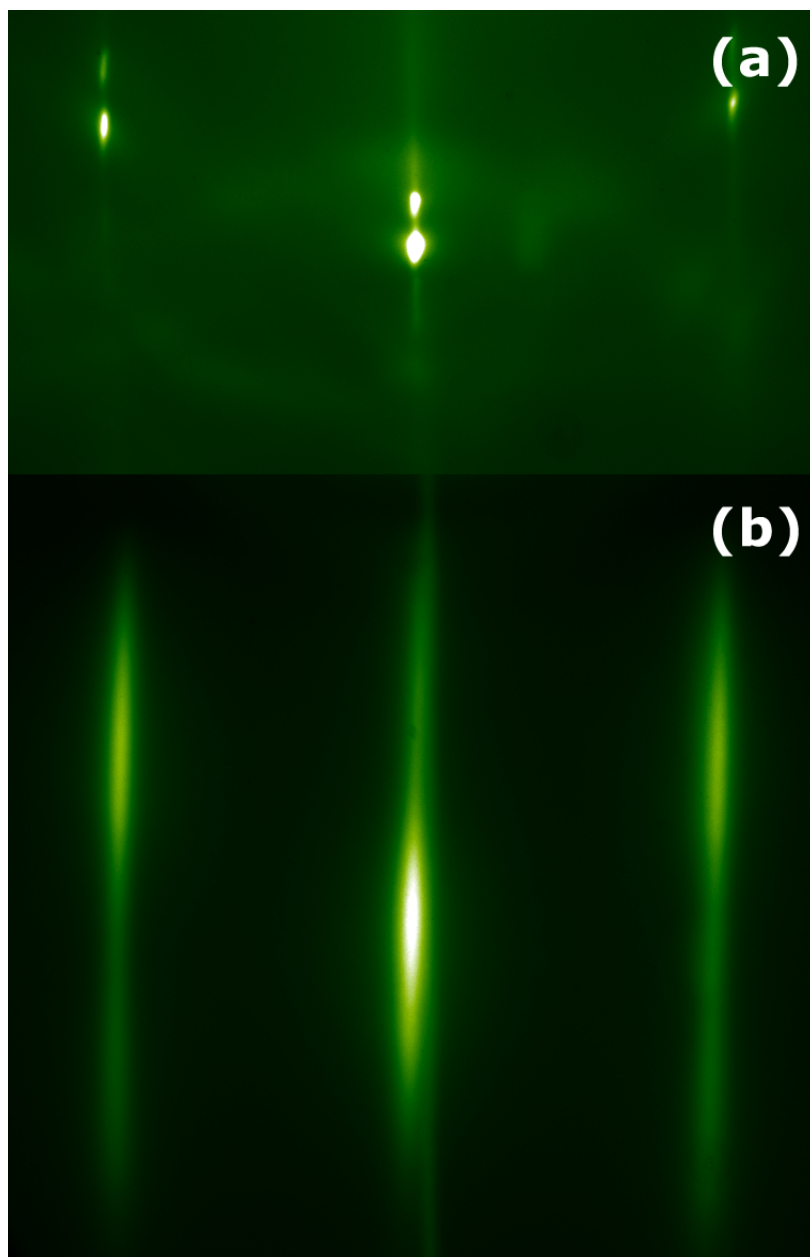


Figure 3.8. RHEED patterns of (a) a bare $(1\bar{1}02)$ Al_2O_3 substrate and (b) a (001) EuO film grown epitaxially upon it. The similar spacing of the vertical streaks in both images indicates that the in-plane lattice spacing of both substrate and film are also similar. There may therefore be hope of growing a coherent EuO film on $(1\bar{1}02)$ Al_2O_3 with biaxial, compressive strain as high as -4%.

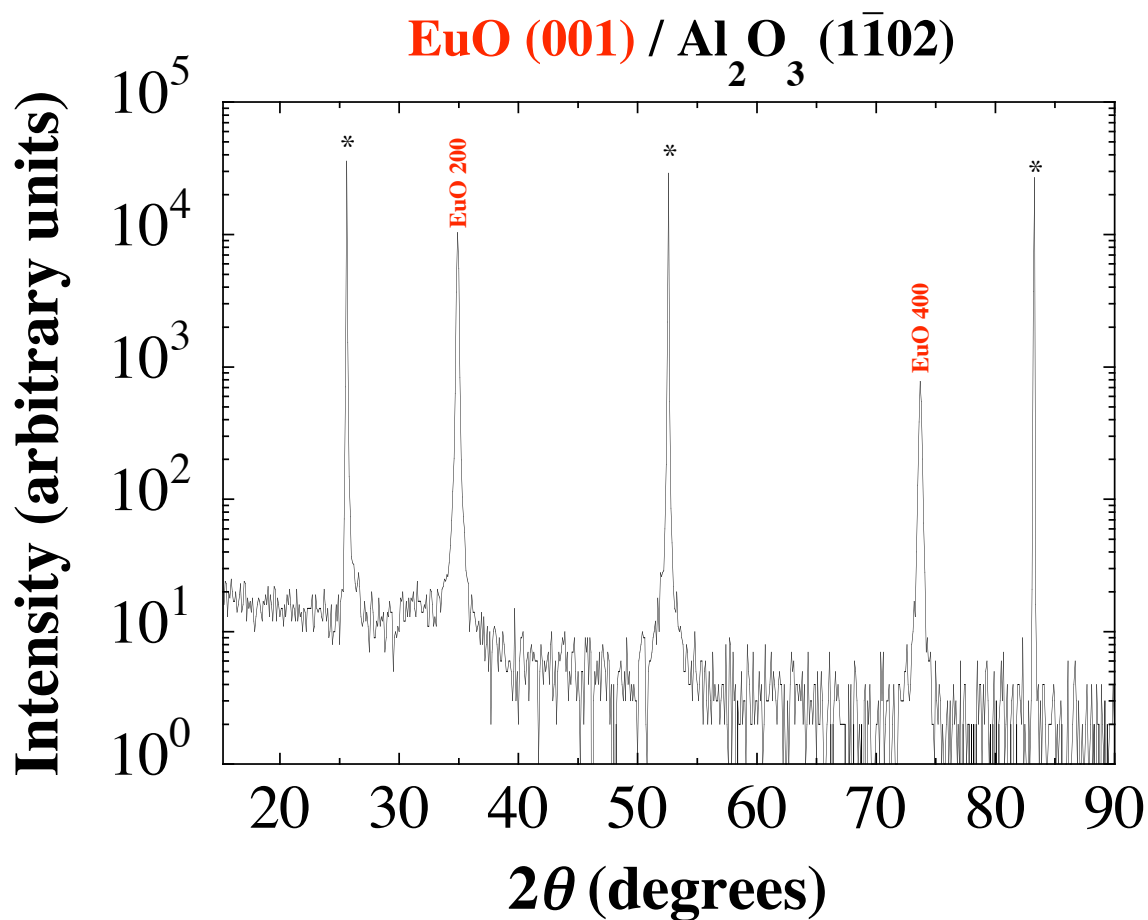


Figure 3.9. XRD pattern of a (001) EuO film grown on $(1\bar{1}02)$ Al_2O_3 . Only the expected peaks are seen, indicating phase purity. This $\theta - 2\theta$ pattern showing the out-of-plane orientation relationship in combination with the RHEED images in Fig. 3.5 revealing the in-plane orientation relationship demonstrates that EuO grows epitaxially on $(1\bar{1}02)$ Al_2O_3 with the following orientation relationship:

$$(001) \text{ EuO} \parallel (1\bar{1}02) \text{ Al}_2\text{O}_3$$

$$[100] \text{ EuO} \parallel [0\bar{1}10] \text{ Al}_2\text{O}_3$$

N-V doped diamond could benefit greatly from injection of spin polarized current directly into its dopant levels by another material. One such material is the highly spin polarized ferromagnetic semiconductor EuO. Here we demonstrate the growth of EuO on diamond. The diamond was grown epitaxially by collaborators in a chemical vapor deposition setup on silicon (35% lattice mismatch).⁴⁰ As grown, the diamond films contain small amounts of (111)-oriented crystallites and rocking curves with FWHM of 6.29° as observed by XRD. Figure 3.10 shows the intensity distribution in 2θ with the diamond and silicon peaks labeled. EuO has a lattice spacing roughly 2% larger than diamond and thus grows epitaxially upon it with relative ease in both (001) EuO / (001) diamond and (111) EuO / (111) diamond orientations. Figure 3.11 shows a XRD ϕ scan of the 111 EuO peaks. These peaks corroborate the four-fold out-of-plane rotation symmetry of cubic EuO and its in-plane epitaxial relationship with the diamond substrate. Figure 3.12 shows the RHEED patterns both the diamond substrate before the EuO film was deposited and the EuO film itself. The orientation of the sample with respect to the RHEED beam was not altered between the two frames. This indicates that the 100 directions of both film and substrate are parallel in-plane. Figures 3.9, 3.10, and 3.11 show that the EuO film is oriented with (001) EuO \parallel (001) diamond out-of-plane and (100) EuO \parallel (100) diamond in-plane. EuO was grown on the aforementioned diamond using the MBE adsorption-controlled method described in chapter two of this thesis. This method allows for the growth of stoichiometric films with comparable quality to the underlying diamond film as evidenced by similar rocking curve FWHM. As grown films even match the (111) oriented impurities found in the underlying (100) diamond films.

As predicted by Ref. 39, the curie temperature of ferromagnetic EuO will increase

under biaxial compressive strain. Because the lattice constant of diamond is 2% smaller than EuO, their epitaxial integration has the added potential of boosting T_c in EuO. The EuO films grown on diamond in this case were not grown coherently with -2% strain and thus no change in T_c was observed.

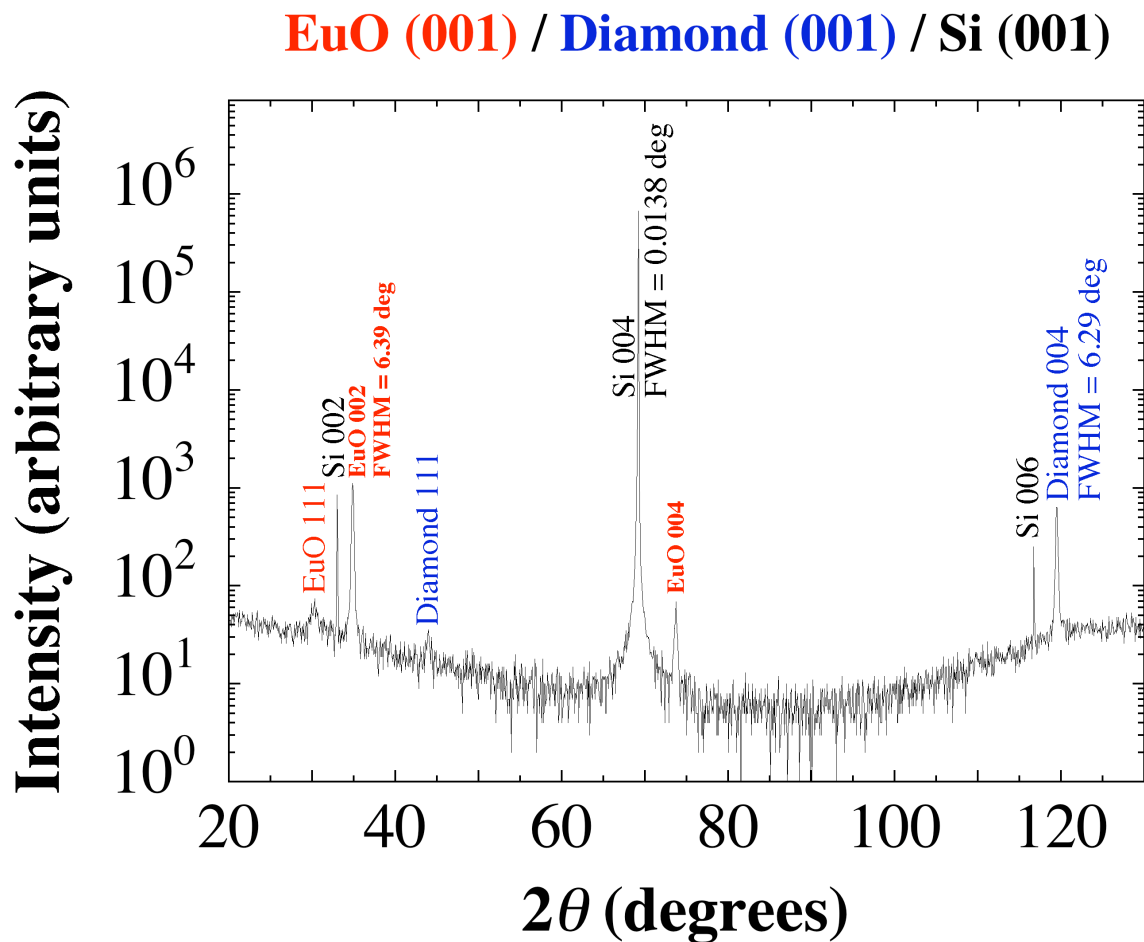


Figure 3.10. XRD intensity distribution of (001) silicon // (001) diamond // (001) EuO in two theta space. In addition to the peaks corresponding to these orientations, 111 diamond can be seen. This acted as a template for the growth of 111 EuO as well.

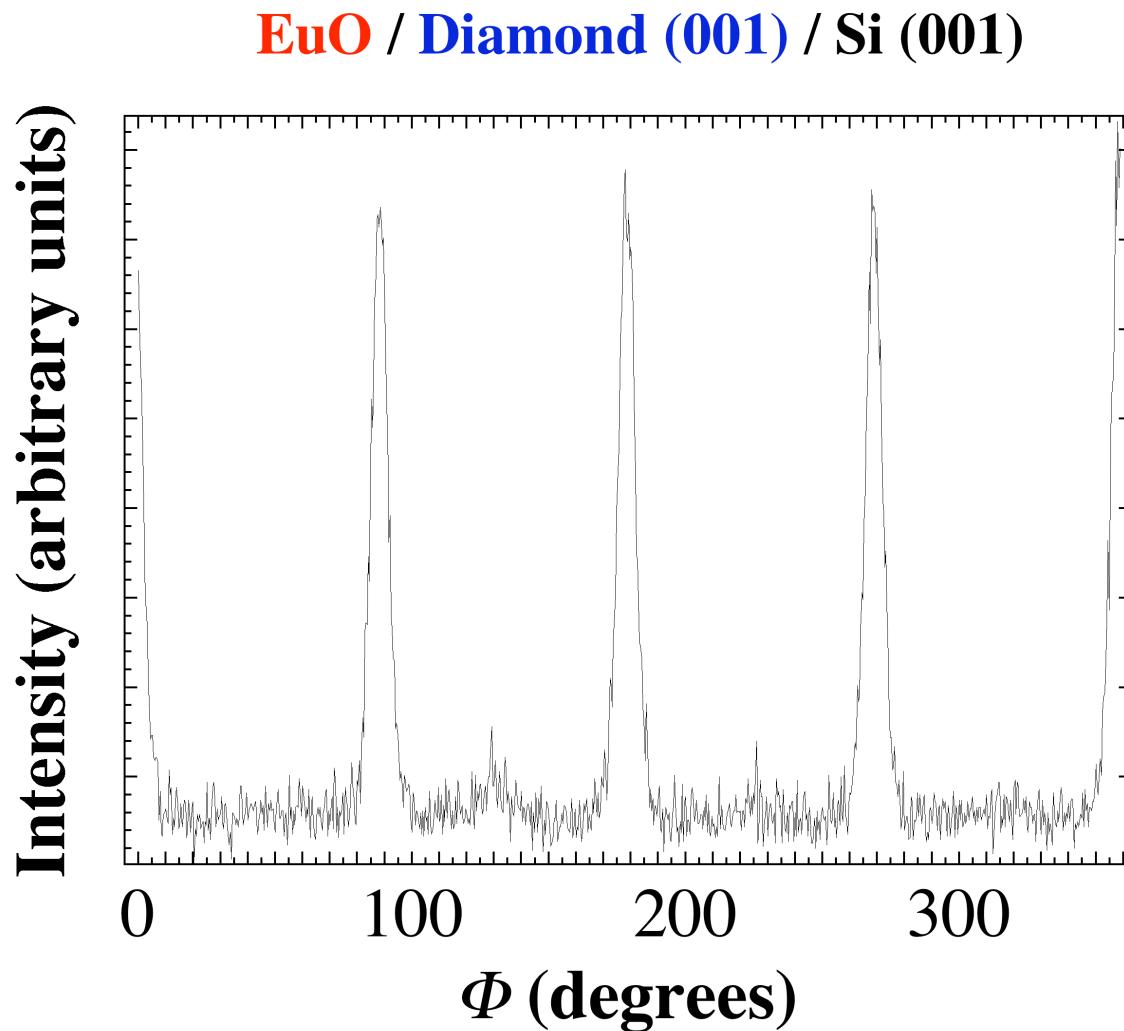


Figure 3.11. Phi scan of the $\{111\}$ family of peaks in 001 oriented EuO. The four peaks seen are indicative of the out of plane, four fold rotation symmetry of cubic EuO. $\Phi = 0$ was set to the 111 peak of the (001) diamond substrate and thus the locations of the 111 EuO peaks above indicate that the 111 EuO directions are oriented in-plane parallel to the 111 diamond directions.

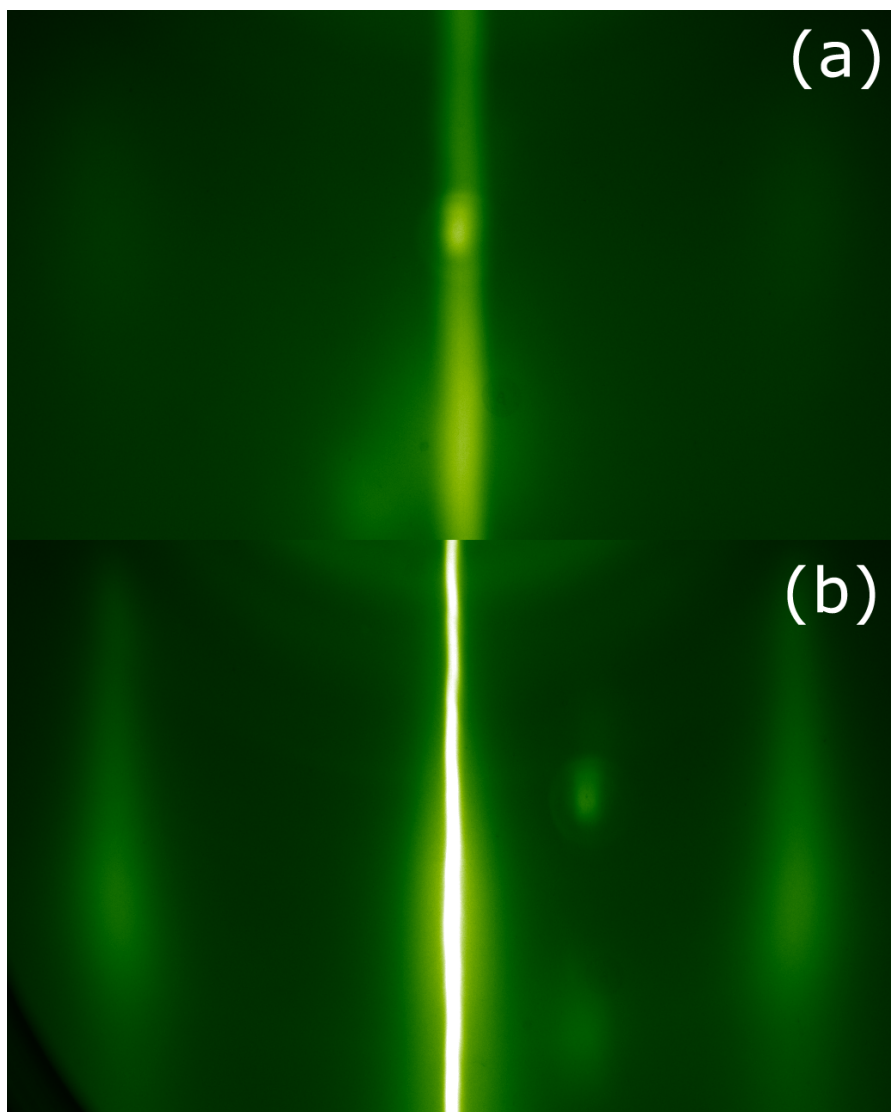


Figure 3.12. RHEED images of (a) a bare (001) diamond substrate and (b) a (001) EuO film grown on top of it. The streak down the middle is due to an imaging error and is not representative of the crystal structure.

Chapter 4: Conclusions and future direction

Though EuO has been synthesized and studied for many decades, recent advances in crystal growth techniques have been utilized to create high quality epitaxial thin films. With its many outstanding properties, it is now receiving attention as a potential component in solid-state spintronic devices. It has also garnered much interest for fundamental research as a prototype Heisenberg ferromagnet.

Here I presented my thesis work on the adsorption-controlled growth of (001) EuO on (110) YAlO_3 , (001) Diamond, (001) LaAlO_3 , and (001) YSZ. EuO grew epitaxially on these materials as evidenced by thorough investigation with high resolution X-Ray Diffraction (XRD) techniques both in and out of the plane of the substrate. (110) YAlO_3 presents a surface net to the growing EuO film 2% larger than its natural lattice spacing. The relaxation thickness of EuO films grown on (110) YAlO_3 was investigated and was found to be 382 ± 25 Å. The thicknesses of various EuO films was determined by RBS and the relaxation thickness was determined by measuring each films rocking curve full width at half maximum and in-plane lattice spacing using XRD. Below the relaxation thickness, commensurate films were found to have rocking curves with full width at half maxima as narrow as 34 arc seconds (0.0097°), the narrowest rocking curves of any reported EuO thin film. The magnetic properties of the best films were measured with a SQUID magnetometer and were found to have a saturation magnetization of $6.96 \pm 0.07 \mu_B/\text{Eu}$, the highest yet reported. High quality films were also obtained by growing on (001) LaAlO_3 and (001) YSZ. Though the EuO films grown on (001) diamond were of much poorer quality, this is a reflection on the quality of the

underlying diamond film and not the EuO film or its growth method because the EuO film quality nearly matched the quality of its diamond substrate which is the limiting factor in the quality of the final film.

Despite the great potential of EuO, there are still substantial challenges that must be overcome before it can be utilized fully. For one, it has a Curie temperature well below room temperature at 69 K. Current work is highly focused upon boosting T_c through compressive strain and doping. It has already been shown that its T_c can be raised through doping via gadolinium substitution and that hydrostatic high pressure can also boost T_c . The highest T_c observed using these methods is 170 K.²³ There is also unpublished evidence also that the concentration of oxygen vacancies could play a role in the doping effect on T_c .⁴⁵ Therefore, future work should be focused on growing commensurate EuO on high quality diamond films to induce a 2% biaxially compressive strain. The effect of oxygen vacancies on T_c should also be investigated by growing EuO films with varying degrees of oxygen vacancies. This can be accomplished using the flux matching technique with oxygen flux tuned in accordance with the adsorption-controlled study presented in chapter 2. Though attempts to integrate EuO with materials that would induce an even larger strain than (001) diamond such as (1 $\bar{1}$ 02) Al_2O_3 (-4% strain) have been made, potential substrates should be sought out and utilized so as to better confirm the effect of strain on T_c and to increase it as far as possible. Though EuO suffers from the fact that it is unstable in air, it has been demonstrated that transmission electron microscopy (TEM) can be used to investigate its crystal structure and eventually this technique should be used to confirm the crystal structure quality and epitaxy beyond the limits of XRD of EuO films grown by the adsorption-controlled method.

REFERENCES

- ¹ F. Levy, *Physik. Kondens. Materie.* **10**, 71 (1969).
- ² G. J. McCarthy, *J. Am. Ceram. Soc.* **57**, 502 (1974).
- ³ J. R. Arthur Jr. *J. Appl. Phys.* **39**, 4032 (1968).
- ⁴ M.A. Herman, H. Sitter, *Molecular Beam Epitaxy* (1996).
- ⁵ Darrell G. Schlom, Long-Qing Chen, Xiaoqing Pan, Andreas Schmehl, and Mark A. Zurbuchen, *J. Am. Ceram. Soc.* **91**, 2429 (2008).
- ⁶ C. D. Theis, J. Yeh, D. G. Schlom, M. E. Hawley, and G. W. Brown, *Thin Solid Films* **325**, 107 (1998).
- ⁷ C. D. Theis, J. Yeh, D. G. Schlom, M. E. Hawley, G. W. Brown, J. C. Jiang, and X. Q. Pan, *Appl. Phys. Lett.* **72**, 22 (1998).
- ⁸ P. G. Steeneken, Ph. D. thesis, Rijksuniversiteit Groningen, 2002.
- ⁹ B. T. Matthias, R. M. Bozorth, and J. H. van Vleck, *Phys. Rev. Lett.* **7**, 160 (1961).
- ¹⁰ Kie Y. Ahn and J. C. Suits, *IEEE Trans. Magn.* **3**, 453 (1967).
- ¹¹ Kenneth Lee and J. C. Suits, *J. Appl. Phys.* **41**, 954 (1970).
- ¹² K. Kawaguchi and M. Sohma, *Thin Solid Films* **246**, 1 (1994).
- ¹³ Guanghua Yi and E. Batalla, *J. Mater. Res.* **11** 2470 (1996).
- ¹⁴ K. Kawaguchi, M. Sohma, Y. Oosawa, *J. Magn. Magn. Mater.* **148**, 80 (1995).
- ¹⁵ Nobuyuki Iwata, Govind Pindoria, Tadaka Morishita, and Kay Kohn, *J. Phys. Soc. Jap.* **69**, 230 (2000).
- ¹⁶ J. C. Suits and Kenneth Lee, *J. Appl. Phys.* **42** 2358 (1971).

-
- ¹⁷ C. Paparoditis, R. Suryanarayanan, C. Llinares, E. Monteil, and G. Bordure, *Solid State Commun.* **9**, 1871 (1971).
- ¹⁸ M. J. Freiser, F. Holtzberg, S. Methfessel, G. D. Petit, M. W. Shafer, and J. C. Suits, *Helv. Phys. Acta* **41**, 832 (1968).
- ¹⁹ A. Schmehl, V. Vaithyanathan, A. Herrnberger, S. Thiel, C. Richter, M. Liberati, T. Heeg, M. Röckerath, L. F. Kourkoutis, S. Mühlbauer, P. Böni, D. A. Muller, Y. Barash, J. Schubert, Y. Idzerda, J. Mannhart, and D. G. Schlom, *Nat. Mater.* **7**, 882 (2007).
- ²⁰ K. Y. Ahn and M. W. Shafer, *J. Appl. Phys.* **41**, 1260 (1970).
- ²¹ M. R. Oliver, J. O. Dimmock, A. L. McWhorter, and T. B. Reed, *Phys. Rev. B* **5**, 1078 (1972).
- ²² G. Petrich, S. von Molnár, and T. Penney, *Phys. Rev. Lett.* **26**, 885 (1971).
- ²³ H. Ott, S. J. Heise, R. Sutarto, Z. Hu, C. F. Chang, H. H. Hsieh, H. J. Lin, C. T. Chen, and L. H. Tjeng, *Phys. Rev. B* **73**, 094407 (2006).
- ²⁴ K. Sattler and H. C. Siegmann, *Phys. Rev. Lett.* **29**, 1565 (1972).
- ²⁵ H. A. Mook, *Phys. Rev. Lett.* **46**, 508 (1981).
- ²⁶ C. Llinares, L. Gousskov, C. Duchemin, and G. Bordure, *J. Phys. Chem. Solids* **36**, 567 (1974).
- ²⁷ N. Iwata, G. Pindoria, T. Morishita, and K. Kohn, *J. Phys. Soc. Jpn.* **69**, 230 (2000).
- ²⁸ P. G. Steeneken, L. H. Tjeng, I. Elfimov, G. A. Sawatzky, G. Ghiringhelli, N. B. Brookes, and D. J. Huang, *Phys. Rev. Lett.* **88**, 047201 (2002).
- ²⁹ J. Lettieri, V. Vaithyanathan, S. K. Eah, J. Stephens, V. Sih, D. D. Awschalom, J. Levy, and D. G. Schlom, *Appl. Phys. Lett.* **83**, 975 (2003).
- ³⁰ K. Lee and J. C. Suits, *J. Appl. Phys.* **41**, 954 (1970).

-
- ³¹ H. Ott, S. J. Heise, R. Sutarto, Z. Hu, C. F. Chang, H. H. Hsieh, H. J. Lin, C. T. Chen, and L. H. Tjeng, *Phys. Rev. B* **73**, 094407 (2006).
- ³² C. D. Theis and D. G. Schlom, *J. Cryst. Growth* **174**, 473 (1997).
- ³³ G. M. Roesler, Jr., Y. U. Idzerda, P. R. Broussard, and M. S. Osofsky, *J. Appl. Phys.* **75**, 6679 (1994).
- ³⁴ R. Diehl and G. Brandt, *Mater. Res. Bull.* **10**, 85 (1975).
- ³⁵ Y. Shapira and T. B. Reed, *AIP Conference Proceedings* **5**, 837 (1971).
- ³⁶ P. F. Miceli and C. J. Palmstrøm, *Phys. Rev. B* **51**, 5506 (1995).
- ³⁷ C. Kim, T. Spila, I. K. Robinson, and J. E. Greene, *J. Appl. Phys.* **83**, 7608 (1998).
- ³⁸ A. R. Kortan, M. Hong, J. Kwo, J. P. Mannaerts, and N. Kopylov, *Phys. Rev. B.* **60**, 10913 (1999).
- ³⁹ N. J. C. Ingle and I. S. Elfimov, *Phys. Rev. B* **72**, 12 (2008).
- ⁴⁰ S. Gsell, T. Bauer, J. Goldfuß, M. Schreck, and B. Strzker, *Appl. Phys. Lett.* **84**, 22 (2004).
- ⁴¹ M. Fischer, S. Gsell, M. Schreck, R. Brescia, B. Strizker, *Dia. Rel. Mat.* (in press).
- ⁴² S. Gsell, M. Fischer, Th. Bauer, M. Schreck, B. Stritzker, *Dia. Rel. Mat.* **15**, 479 (2006).
- ⁴³ R. J. Epstein, F. M. Mendoza, Y. K. Kato, and D. D. Awschalom, *Nat. Phys.* **1**, 94 (2005).
- ⁴⁴ R. Hanson, F. M. Mendoza, R. J. Epstein, and D. D. Awschalom, *Phys. Rev. Lett.* **97**, 087601 (2006).
- ⁴⁵ Private communication (Andreas Schmehl).